Lawrence Berkeley National Laboratory

Title
Dielectron production in proton-proton collisions at s=7 TeV

Authors
The ALICE collaboration
Acharya, S
Acosta, F T-
et al.

Dielectron production in proton-proton collisions at $\sqrt{s} = 7$ TeV

The ALICE collaboration

E-mail: ALICE-publications@cern.ch

ABSTRACT: The first measurement of e^+e^- pair production at mid-rapidity ($|\eta_e| < 0.8$) in pp collisions at $\sqrt{s} = 7$ TeV with ALICE at the LHC is presented. The dielectron production is studied as a function of the invariant mass ($m_{ee} < 3.3$ GeV/c^2), the pair transverse momentum ($p_{T,ee} < 8$ GeV/c), and the pair transverse impact parameter (DCA$_{ee}$), i.e., the average distance of closest approach of the reconstructed electron and positron tracks to the collision vertex, normalised to its resolution. The results are compared with the expectations from a cocktail of known hadronic sources and are well described when PYTHIA is used to generate the heavy-flavour contributions. In the low-mass region ($0.14 < m_{ee} < 1.1$ GeV/c^2), prompt and non-prompt e^+e^- sources can be separated via the DCA$_{ee}$. In the intermediate-mass region ($1.1 < m_{ee} < 2.7$ GeV/c^2), a double-differential fit to the data in m_{ee} and $p_{T,ee}$ and a fit of the DCA$_{ee}$ distribution allow the total $c\bar{c}$ and $b\bar{b}$ cross sections to be extracted. Two different event generators, PYTHIA and POWHEG, can reproduce the shape of the two-dimensional m_{ee} and $p_{T,ee}$ spectra, as well as the shape of the DCA$_{ee}$ distribution, reasonably well. However, differences in the $c\bar{c}$ and $b\bar{b}$ cross sections are observed when using the generators to extrapolate to full phase space. Finally, the ratio of inclusive to decay photons is studied via the measurement of virtual direct photons in the transverse-momentum range $1 < p_T < 8$ GeV/c. This is found to be unity within the statistical and systematic uncertainties and consistent with expectations from next-to-leading order perturbative quantum chromodynamic calculations.

Contents

1 Introduction

The main goal of the ALICE [1–3] Collaboration is to study strongly-interacting matter at the high energy density and temperature reached in ultra-relativistic heavy-ion collisions at the CERN Large Hadron Collider (LHC). In such collisions, the formation of a deconfined state of quarks and gluons, the Quark−Gluon Plasma (QGP), is predicted by Quantum ChromoDynamic (QCD) calculations on the lattice [4–8]. Moreover, chiral symmetry is expected to be restored in the QGP phase [9, 10].

Electron-positron pairs are produced at all stages of the collision. Since they are not affected by the strong interaction, they can escape from the dense medium without final-state interaction, and are suited to probe the entire time evolution and dynamics of the

system. At low invariant masses of the dielectron pairs ($m_{ee} < 1.1\,\mathrm{GeV}/c^2$), e^+e^- spectra are sensitive to the properties of vector mesons ρ, ω, and ϕ in the medium. The ρ meson has a shorter lifetime ($\approx 1.3\,\mathrm{fm}/c$ in its rest frame) than that of the medium ($\approx 10\,\mathrm{fm}/c$ [11]). Therefore, its spectral function, which can be measured through its dielectron decay channel, is affected by the dense medium and the predicted restoration of chiral symmetry [12–14]. Thermal radiation emitted by the system, both during the partonic and hadronic phase [9, 10], contributes to the dielectron yield over a broad mass range. In the intermediate-mass region (IMR, $1.1 < m_{ee} < 2.7\,\mathrm{GeV}/c^2$), the measurement of thermal dielectrons from the QGP is very challenging at the LHC due to the dominant contribution of e^+e^- pairs from semileptonic decays of charm and beauty hadrons, correlated through flavour conservation.[1] The continuum produced by these decays is sensitive to the energy loss [15–19] and the degree of thermalisation of charm and beauty quarks in the medium, as well as the heavy-quark hadronisation mechanism, e.g. recombination of heavy quarks with light quarks from the thermalised medium [20–22]. To single out the interesting signal characteristics of the QGP, it is crucial to understand the dielectron yield from primordial heavy-flavour production. The latter can be studied in proton-proton (pp) collisions, which serve as a reference for the analysis of heavy-ion collisions and provide a test for perturbative QCD (pQCD) calculations and Monte Carlo (MC) event generators. Complementary to single-electron or D meson measurements, the yield of correlated e^+e^- pairs from charm-hadron decays contains information about kinematical correlations between the c and $\bar{\mathrm{c}}$ quarks, i.e. the production mechanisms, and is sensitive to soft heavy-flavour production.

At the Relativistic Heavy Ion Collider (RHIC), the PHENIX and STAR Collaborations found that the dielectron production in pp collisions at $\sqrt{s} = 200\,\mathrm{GeV}$ is well described by a cocktail of expected hadronic sources [23–25]. In addition, PHENIX measured the total $c\bar{c}$ and $b\bar{b}$ cross sections in pp and d-Au collisions at $\sqrt{s_{\mathrm{NN}}} = 200\,\mathrm{GeV}$ by fitting the spectra of e^+e^- pairs from heavy-flavour hadron decays simultaneously in m_{ee} and pair transverse momentum $p_{\mathrm{T,ee}}$ [26, 27]. At this energy and in the PHENIX acceptance, the yield from correlated pairs from beauty-hadron decays dominates across all mass regions for $p_{\mathrm{T,ee}} > 2.5\,\mathrm{GeV}/c$, whereas the $c\bar{c}$ contribution is preeminent for $m_{ee} < 3\,\mathrm{GeV}/c^2$ and $p_{\mathrm{T,ee}} < 2\,\mathrm{GeV}/c$. The extraction of the heavy-flavour cross sections, in particular the total $c\bar{c}$ cross section, depends nevertheless on the event generator used to extrapolate the measurements to full phase space. Finally, at lower masses ($m_{ee} < 0.3\,\mathrm{GeV}/c^2$) and high $p_{\mathrm{T,ee}}$ ($p_{\mathrm{T,ee}} > 1\,\mathrm{GeV}/c$), i.e. the quasi-real virtual-photon region where the $p_{\mathrm{T,ee}}$ of the dilepton pair is much larger than its mass ($p_{\mathrm{T,ee}}^2 \gg m_{ee}^2$), the measured e^+e^- yield was used to study the production of virtual direct photons. The corresponding yield of real direct photons in pp and d-Au collisions is reproduced by next-to-leading order perturbative quantum chromodynamic (NLO pQCD) calculations [24, 28]. At the LHC, no significant signal of direct photons for $p_{\mathrm{T}} < 16\,\mathrm{GeV}/c$ could be extracted from the inclusive photon measurements in pp collisions at $\sqrt{s} = 2.76\,\mathrm{TeV}$ and $8\,\mathrm{TeV}$ by the ALICE Collaboration [29]. However, the results are consistent with expectations from NLO pQCD calculations, which predict a smaller contribution of direct photons to the inclusive photon spectrum with increasing $\sqrt{s}$.

---

[1]These contributions are referred to as charm/beauty or $c\bar{c}$/$b\bar{b}$ contributions throughout this paper.

In heavy-ion collisions, a strong enhancement at low invariant mass of dilepton pairs ($m_{ll} < 1\,\mathrm{GeV}/c^2$) is observed at different energies, at the Super Proton Synchroton (SPS) by the CERES and NA60 Collaborations [30–35] and at RHIC energies by the PHENIX and STAR Collaborations [24, 36–38]. The data can be explained by thermal radiation of the hadronic phase, dominated by the ρ meson, which appears strongly broadened [39–47] with essentially no change of the pole mass. This broadening is consistent with chiral symmetry restoration [14]. At RHIC, the data show a further excess of the direct-photon yield over the pp expectation, which is exponential in p_{T} with an inverse slope T of about $221\,\mathrm{MeV}$ [24]. This excess can be attributed to thermal radiation from the partonic and/or hadronic phase [46, 48, 49]. At the LHC, a similar enhancement of the direct-photon production, with $T \approx 297\,\mathrm{MeV}$, is observed in central Pb-Pb collisions at $\sqrt{s_{\mathrm{NN}}} = 2.76\,\mathrm{TeV}$ [50]. In the IMR, a significant excess over the yield from semileptonic decays of heavy-flavour hadrons is found at the SPS [34, 35, 51, 52], whereas at RHIC the data can be fairly well described by calculations including heavy-flavour contributions estimated in pp collisions and scaled with the number of binary collisions [24, 36–38]. At the SPS, the NA60 Collaboration showed, by using precise vertex information, that the excess is associated with a prompt source, as opposed to $\mu^+\mu^-$ pairs from D mesons that decay further away from the interaction point [51]. The analysis of the $p_{\mathrm{T},\mu\mu}$-spectra, with the extraction of the slope parameter T_{eff} as a function of $m_{\mu\mu}$, revealed that the IMR is dominated by an early source of dileptons, i.e. partonic radiation, where radial flow is negligible [52]. Models including thermal radiation from the QGP [39, 41, 42, 53] can reproduce the data in the IMR.

In this paper, the first measurement of the e^+e^- pair production in pp collisions at $\sqrt{s} = 7\,\mathrm{TeV}$ with ALICE at the LHC is presented. The invariant yield is studied within the central barrel acceptance of ALICE ($|\eta_{\mathrm{e}}| < 0.8$) as a function of m_{ee} ($m_{\mathrm{ee}} < 3.3\,\mathrm{GeV}/c^2$), $p_{\mathrm{T,ee}}$ ($p_{\mathrm{T,ee}} < 8\,\mathrm{GeV}/c$), and $\mathrm{DCA}_{\mathrm{ee}}$ ($\mathrm{DCA}_{\mathrm{ee}} < 10\,\sigma$), i.e. the average distance of closest approach of the reconstructed electron and positron tracks to the collision vertex, normalised to its resolution. The latter allows the prompt and non-prompt dielectron sources to be separated and provides an additional variable to disentangle the contributions from $c\bar{c}$ (with $c\tau \approx 150\,\mu\mathrm{m}$ for D mesons) and $b\bar{b}$ (with $c\tau \approx 470\,\mu\mathrm{m}$ for B mesons). The data are compared with a cocktail of expected e^+e^- sources from known hadrons based on measured cross sections. Correlated pairs from heavy-flavour hadron decays are calculated with two different MC event generators, PYTHIA [54] and POWHEG [55–58]. Finally, the relative contribution of virtual direct photons is shown and compared with NLO pQCD calculations.

This article is organised as follows: the experimental apparatus and data sample used in the analysis are presented in section 2. The analysis strategy, including the electron identification, the background subtraction, and the efficiency corrections are described in section 3, together with the associated systematic uncertainties. In section 4, the procedures used to calculate the expected dielectron cross section from the known hadronic sources are explained. The results, i.e. the invariant mass spectrum, the $p_{\mathrm{T,ee}}$ and $\mathrm{DCA}_{\mathrm{ee}}$ distributions, are finally presented and discussed in section 5. In the same section, the charm and beauty total cross sections, as well as the fraction of direct photons to inclusive photons, are extracted from the data.

2 Experimental apparatus and data sample

The ALICE apparatus and its performance are described in detail in [1–3, 59]. In the following, only the subsystems relevant for the dielectron analysis are briefly discussed. Electrons[2] are reconstructed and identified at mid-rapidity ($|\eta_e| < 0.8$) in the central barrel of ALICE with the Inner Tracking System (ITS), the Time Projection Chamber (TPC), and the Time-Of-Flight system (TOF). These detectors are located inside a large solenoidal magnet that provides a uniform magnetic field of $B = 0.5$ T along the beam direction.

The ITS [60] is the detector closest to the beam axis. It is composed of six cylindrical layers of silicon detectors, with radial distances ranging from 3.9 cm to 43 cm. The two innermost layers are equipped with Silicon Pixel Detectors (SPD). The two intermediate layers consist of Silicon Drift Detectors (SDD), and the two outermost layers are made of Silicon Strip Detectors (SSD). The high spatial resolution of the silicon sensors allows the Distance-of-Closest-Approach (DCA) of the track to the reconstructed collision vertex (primary vertex) to be measured. The DCA resolution in the plane transverse to the beam direction is better than 75 μm for charged particles with transverse momenta $p_T > 1$ GeV/c. Moreover, the four SDD and SSD layers provide charged-particle identification via the measurement of their specific energy loss dE/dx.

At larger radii ($85 < r < 247$ cm), a 500 cm long cylindrical TPC [61] provides identification of charged particles and reconstruction of their trajectories. Up to 159 three-dimensional space points per track, which corresponds to the number of pad rows in one TPC sector out of 18 in azimuth, are recorded and used to estimate the dE/dx of charged particles in the gas. The dE/dx resolution in pp collisions is about 5.2% for minimum-ionising particles passing through the full detector [59].

The charged-particle identification capability of the TPC and ITS is supplemented by the TOF [62], which is located at a radial distance of 3.7 m from the beam axis. It provides a measurement of the time of flight for particles from the interaction point up to the detector itself. The event collision time is either measured with the T0 detector, which consists of two arrays of Cherenkov counters located at $z = +375$ cm and $z = -72.7$ cm from the nominal interaction point, or estimated using the particle arrival times at the TOF for events with sufficiently large multiplicity [59]. Due to their curved paths in the magnetic field of the solenoidal magnet, charged particles need a minimum p_T of about 300 MeV/c to reach the TOF detector. Since the TOF matching efficiency is of the order of 30% at a p_T of 500 MeV/c, the TOF information is used in this analysis only if the particle has an associated hit in the TOF detector, otherwise the particle is identified with the ITS and TPC only.

The V0 detector [63], used for triggering, consists of two arrays of 32 scintillators each, placed around the beam vacuum tube on either side of the interaction region at $z = -90$ cm and $z = +340$ cm. The two arrays cover the pseudorapidity ranges $2.8 < \eta < 5.1$ (V0A) and $-3.7 < \eta < -1.7$ (V0C), respectively.

The data used in this paper were recorded with ALICE at the LHC during the pp run at $\sqrt{s} = 7$ TeV in 2010. Minimum bias (MB) collisions were triggered by requiring at least one hit in the SPD or in one of the two forward scintillator systems V0A and V0C.

---

[2]The term 'electron' is used for both electrons and positrons throughout this paper.

In addition, the timing information from the V0 and the correlation between the number of hits and track segments in the SPD detector were used offline to remove background from beam-gas interactions. The primary vertex is reconstructed by extrapolating charged-particle tracks in the TPC and ITS to the beam line. It is required to be within $\pm 10\,\mathrm{cm}$ of the nominal interaction point along the beam direction in order to provide a uniform pseudo-rapidity acceptance of the detectors. A total of 370 million pp events at $\sqrt{s} = 7\,\mathrm{TeV}$ pass the offline event selection criteria, corresponding to an integrated luminosity of $L_{\mathrm{int}} = (6.0 \pm 0.2)\,\mathrm{nb}^{-1}$ [64].

3 Data analysis

3.1 Electron identification

The strategy to identify electrons relies on a combination of tracking and particle identification (PID) information from different detectors in the central barrel. Reconstructed charged-particle tracks in the ITS and TPC are selected in $|\eta| < 0.8$ and $p_{\mathrm{T}} > 0.2\,\mathrm{GeV}/c$. For the DCA$_{\mathrm{ee}}$ analysis, the tracks must have a $p_{\mathrm{T}} > 0.4\,\mathrm{GeV}/c$ to assure a sufficient separation between prompt and non-prompt $\mathrm{e}^+\mathrm{e}^-$ sources. The DCA resolution worsens at low p_{T} and is larger than $150\,\mu\mathrm{m}$ for tracks reconstructed in the ITS and TPC with $p_{\mathrm{T}} < 0.35\,\mathrm{GeV}/c$ [59], which is of the same order of magnitude as the decay length of the D^0 and $\mathrm{D}_{\mathrm{s}}^{\pm}$ mesons ($c\tau \approx 122.9$ and $149.9\,\mu\mathrm{m}$, respectively). The tracks are required to have at least 100 out of a maximum of 159 reconstructed space points in the TPC with at least 100 crossed pad-rows, while the ITS track segments must have a hit in at least 5 of the 6 detector layers. The maximum χ^2 per space point in the TPC (ITS) from the track fit must be less than 4 (4.5). Only tracks with a DCA to the primary vertex smaller than 1 cm in the xy-plane and 3 cm along the z-axis are accepted. To suppress electron tracks from photon conversions in the detector material at large radii, a hit in the first layer of the SPD is required. This rejects about 63% of the conversion electron tracks, keeping 83% of the signal electrons from light and heavy-flavour hadron decays. A small fraction of electrons from photon conversions in the second ITS layer may still have a hit in the first layer associated wrongly to their reconstructed track. Such cases are further removed from the sample by requiring that the reconstructed track does not share any ITS cluster with other tracks (see below). This requirement also reduces the amount of conversion electrons from the first ITS layer, rejecting 38% of the remaining conversion contamination after the requirement of a hit in the first SPD layer and keeping 97% of the signal electrons. For $\mathrm{e}^+\mathrm{e}^-$ pairs from photon conversions, where both electrons pass the default track selection, the rejection factor is even higher, about 92%.

The PID information is based on the measurement of the specific ionisation energy loss ($\mathrm{d}E/\mathrm{d}x$) in the TPC and ITS, and the time-of-flight information from TOF. The cut values for electron selection and hadron rejection are expressed in terms of the deviation of the respective PID signal from its expectation value for a particle species i. The PID variables $n_{\sigma_{\mathrm{i}}}^{\mathrm{DET}}$ are normalised to units of standard deviations of the respective detector (DET) resolution.
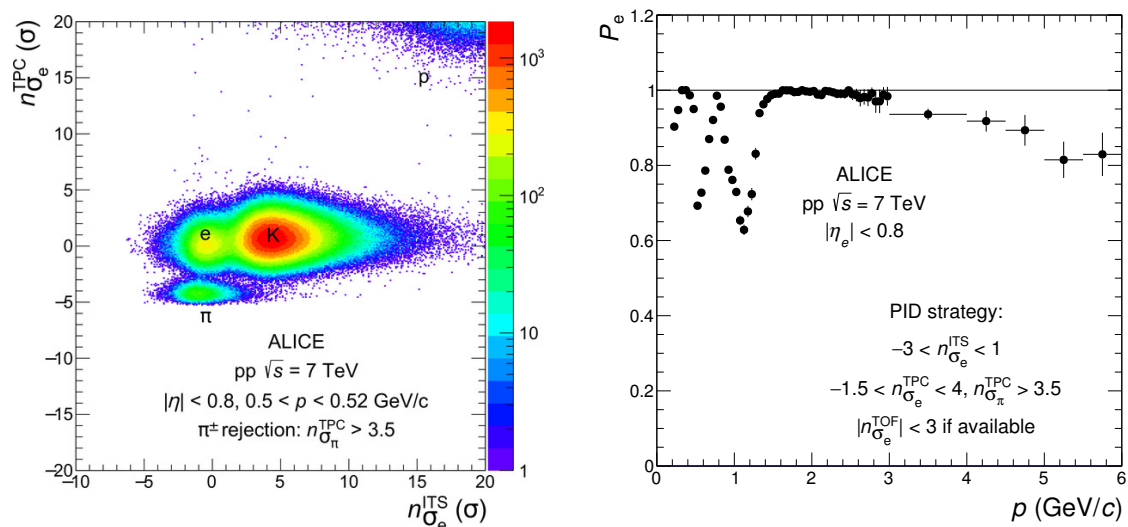
Figure 1. (Colour online) TPC PID signal expressed as $n_{\sigma_e}^{\rm TPC}$ (see text) as a function of the ITS PID signal ($n_{\sigma_e}^{\rm ITS}$) for selected tracks with $0.5 < p < 0.52\,{\rm GeV}/c$ after applying the pion rejection in the TPC (left). Electron purity P_e as a function of momentum (right). Only statistical uncertainties are shown.

In the TPC, electrons are selected in the interval $-1.5 < n_{\sigma_e}^{\rm TPC} < 4.0$. Additionally, pions are rejected by requiring that the measured TPC dE/dx of the track is far from the expectation value for pions: $n_{\sigma_\pi}^{\rm TPC} > 3.5$. Since electrons have a larger energy loss in the TPC than pions for momenta above $0.25\,{\rm GeV}/c$, the $n_{\sigma_\pi}^{\rm TPC}$ requirement is asymmetric. The remaining contamination by kaons and protons occurs mainly in the crossing regions of the expected dE/dx values in the TPC for these particle species and for electrons, i.e. around a momentum of 0.5 and $1.1\,{\rm GeV}/c$, respectively. This contamination can be reduced by using the ITS information, where the crossings occur at higher momenta around 0.7 and $1.5\,{\rm GeV}/c$ for kaons and protons, respectively. In the left panel of figure 1, the variable $n_{\sigma_e}^{\rm TPC}$ is shown as a function of $n_{\sigma_e}^{\rm ITS}$ for selected tracks with $0.5 < p < 0.52$ ${\rm GeV}/c$ after the pion rejection in the TPC was applied. In this momentum interval, kaons and electrons have a very similar energy loss in the TPC, whereas they are still separated in the energy loss measurements of the ITS. The electron selection criterion in the ITS is $-3 < n_{\sigma_e}^{\rm ITS} < 1$. Further reduction of the hadron contamination can be achieved using the TOF information with $|n_{\sigma_e}^{\rm TOF}| < 3$ (in case the selected tracks have an associated hit in the TOF detector). The electron purity P_e is estimated at low momenta ($p < 3\,{\rm GeV}/c$) by fitting the $n_{\sigma_e}^{\rm TPC}$ distribution in momentum slices after the ITS and TOF selection, as well as the $n_{\sigma_\pi}^{\rm TPC}$ rejection, following a procedure explained in [65]. At higher momenta, the $n_{\sigma_\pi}^{\rm TPC}$ distribution is fitted after the requirements on $n_{\sigma_e}^{\rm ITS}$, $n_{\sigma_e}^{\rm TOF}$, and $n_{\sigma_e}^{\rm TPC}$, are fulfilled. The result is shown in the right panel of figure 1. The purity ranges from 60% to 99%, depending on the particle momentum p. The lowest purity is observed where kaons ($p \approx 0.5\,{\rm GeV}/c$) or protons ($p \approx 1.2\,{\rm GeV}/c$) have similar dE/dx as electrons in the TPC.
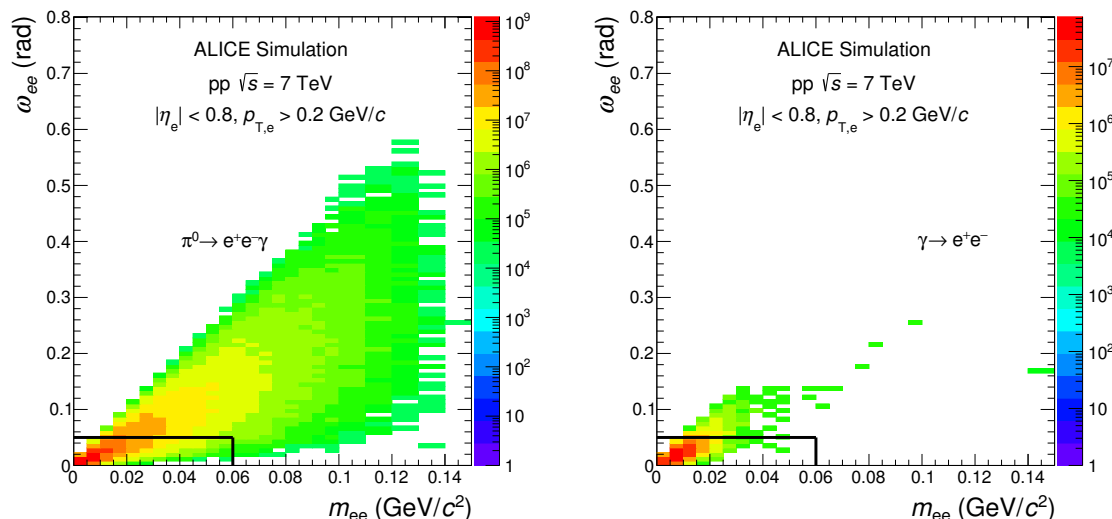
Figure 2. (Colour online) Opening angle vs invariant mass of e^+e^- pairs from π^0 Dalitz decays (left) and from photon conversions (right) in MC simulations after the single track selection criteria. The lines indicate the prefilter requirement.

3.2 Dielectron spectrum

All electron candidates from the same event are combined into pairs, characterised by their m_{ee}, $p_{T,ee}$, and DCA_{ee}. The latter is calculated from the single-electron DCAs as:

$$DCA_{ee} = \sqrt{\frac{(DCA_{xy,1}/\sigma_{xy,1})^2 + (DCA_{xy,2}/\sigma_{xy,2})^2}{2}}, \qquad (3.1)$$

where $DCA_{xy,i}$ is the DCA of the electron i in the transverse plane and $\sigma_{xy,i}$ is its resolution estimated from the covariance matrix of the track reconstruction parameters obtained with the Kalman filter technique [59, 66]. The absolute DCA resolution worsens at low p_T due to multiple scattering in the detector material. Therefore, the analysis is performed using the DCA normalised to its resolution, which decreases the sensitivity to the particle momentum.

The distribution of same-event pairs of opposite sign (OS) is composed of true signal pairs (S) as well as background pairs (B). The background pairs are mainly combinatorial but contain also residual correlations such as from jets and from conversions of correlated decay photons originating from the same mother particle. Typical values of S/B range between $O(1)$ and $O(10^{-1})$, depending on m_{ee} and $p_{T,ee}$ (see below). Therefore, the minimisation of B and a careful subtraction of the remaining background are key aspects of this analysis.

The main sources of electrons contributing to B are π^0 Dalitz decays and photon conversions. To reject these most efficiently, a prefilter algorithm is applied where tracks from the selected electron candidate sample are combined with charged-particle tracks from a sample with relaxed tracking selection criteria and no PID. Dielectron pairs originating from π^0 Dalitz decays and photon conversions have small invariant masses and opening angles (ω_{ee}), as shown in figure 2. Therefore, if an opposite-sign pair with small invariant
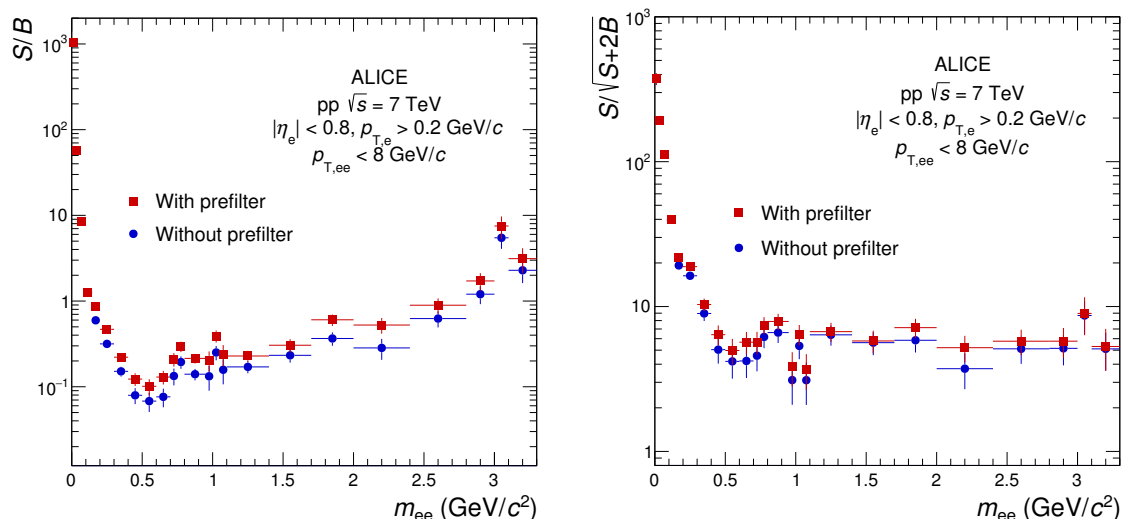
Figure 3. Signal to background ratio (left) and significance (right) obtained with and without applying the prefilter. Only statistical uncertainties are shown. The background is estimated as explained in the text later.

mass and opening angle is formed with a track h of the sample with relaxed selection criteria, the electron candidate is rejected and not used for further pairing. The cut values applied in the prefilter algorithm are $m_{\text{eh}} < 0.06\,\text{GeV}/c^2$ and $\omega_{\text{eh}} < 50$ mrad. These selection criteria lead to an improvement of the S/B by a factor of about 1.5 and an increase of the significance $S/\sqrt{S + 2B}$ by a factor of about 1.2 for $m_{\text{ee}} < 1\,\text{GeV}/c^2$, as can be seen in the left and right panels of figure 3, respectively. For $m_{\text{ee}} < 0.06\,\text{GeV}/c^2$, the prefilter algorithm cuts systematically into the signal acceptance. Since the S/B is large in the low-mass region, no prefilter is applied for $m_{\text{ee}} < 0.14\,\text{GeV}/c^2$. The random rejection probability, caused by accidental combinations of electron candidates with an uncorrelated track, is small (about 3%) and taken into acount in the efficiency corrections.

To further suppress the contamination by dielectron pairs from photon conversions in the dielectron yield, two additional selection criteria are applied. Conversions occur in the beam pipe or in the detector material, mainly of the ITS, and are characterised by a common secondary vertex of the dielectron pair. Any electron candidate found to form such a secondary vertex with another track is rejected from the analysis. In addition, dielectron pairs from photon conversions are characterised by a finite apparent invariant mass. The extrapolation of displaced conversion electron tracks to the collision point results in a non-vanishing artificial opening angle that is caused by the deflection of the tracks in the magnetic field. The opening angle is preferentially in the plane perpendicular to the magnetic field direction, which can be used to further reject such conversion dielectron pairs [24]. To this end, the angle φ_{v} which measures the orientation of the opening angle relative to the magnetic field is calculated according to:

$$\cos(\varphi_{\text{v}}) = \frac{\mathbf{w} \cdot \mathbf{u_a}}{|\mathbf{w}||\mathbf{u_a}|}. \tag{3.2}$$

The two vectors $\mathbf{w}$ and $\mathbf{u_a}$ are given by:

$$\mathbf{w} = \mathbf{u} \times \mathbf{v}, \tag{3.3}$$

$$\mathbf{u_a} = \frac{\mathbf{u} \times \mathbf{z}}{|\mathbf{u} \times \mathbf{z}|}, \tag{3.4}$$

$$\mathbf{u} = \frac{\mathbf{p}_{\mathrm{e}+} + \mathbf{p}_{\mathrm{e}-}}{|\mathbf{p}_{\mathrm{e}+} + \mathbf{p}_{\mathrm{e}-}|}, \tag{3.5}$$

$$\mathbf{v} = \frac{\mathbf{p}_{\mathrm{e}+} \times \mathbf{p}_{\mathrm{e}-}}{|\mathbf{p}_{\mathrm{e}+} \times \mathbf{p}_{\mathrm{e}-}|}, \tag{3.6}$$

where $\mathbf{p}_{\mathrm{e}+}$, $\mathbf{p}_{\mathrm{e}-}$, and $\mathbf{z}$ are the 3-momentum vectors of the positron, electron, and the orientation of the magnetic field parallel to the beam axis, respectively. In the left panel of figure 4, the measured φ_{v} distribution without ITS shared-cluster cut for $m_{\mathrm{ee}} < 0.1\,\mathrm{GeV}/c^2$ and $p_{\mathrm{T,ee}} < 8\,\mathrm{GeV}/c$ is compared with the sum of two MC templates, one for pairs from π^0 and η Dalitz decays and one for pairs from photon conversions, fitted to the data. Prompt pairs with finite invariant mass have an almost uniform φ_{v} distribution in this kinematic domain, while conversion pairs show a peak around $\varphi_{\mathrm{v}} = \pi$. To reject these conversions, reconstructed electron tracks that share at least one ITS cluster with another track are not used in the analysis. The measured φ_{v} distribution after this requirement is shown in the right panel of figure 4. The conversion peak around $\varphi_{\mathrm{v}} = \pi$ is clearly suppressed. The MC simulations describe the data very well. Moreover, dielectron pairs with $\varphi_{\mathrm{v}} > 2$ rad and $m_{\mathrm{ee}} < 0.1\,\mathrm{GeV}/c^2$ are removed from the selected pairs to further reduce the amount of conversion electrons. From MC studies, their final contribution is expected to be below 1% down to $m_{\mathrm{ee}} = 0$.

The remaining background B is estimated from the distribution of same-sign pairs, SS, from the same event. In comparison to a mixed-event approach, the same-sign approximation of the combinatorial background has the advantage of containing all residual correlations arising from charge-symmetric processes such as jet fragmentation or conversions of decay photons from the same mother particle that are present in B, but the disadvantage of suffering from the limited statistics available in the analysed data sample. The same-sign distribution SS is computed in the same bins of m_{ee}, $p_{\mathrm{T,ee}}$, and $\mathrm{DCA_{ee}}$ as the OS distributions by forming in each bin the geometric mean $SS = 2 \cdot \sqrt{N_{++}N_{--}}$ of the number of $(++)$ and $(--)$ pairs, N_{++} and N_{--}, respectively. The geometric mean is robust against charge asymmetries in the electron sample, as they may arise from acceptance differences of positive and negative tracks, and from charge asymmetries of the hadronic background. In the present data set, charge asymmetries of up to 5% are observed, depending on p_{T}. MC simulations confirm that such asymmetries do not lead to a bias in the estimate of B if the geometric mean is used for the same-sign background calculation. In a few bins with low pair statistics, however, N_{++} or N_{--} is zero. In such bins, the arithmetic sum $SS = N_{++} + N_{--}$ is used instead, to avoid underestimation of the combinatorial background.

A bias in the estimate of B using the same-sign technique can occur as a consequence of differences of the detector acceptance for same-sign and opposite-sign pairs. Due to the full coverage of the ALICE central barrel in azimuth, i.e. in the bending plane of the spectrometer, such acceptance differences are small. Residual effects arise due to
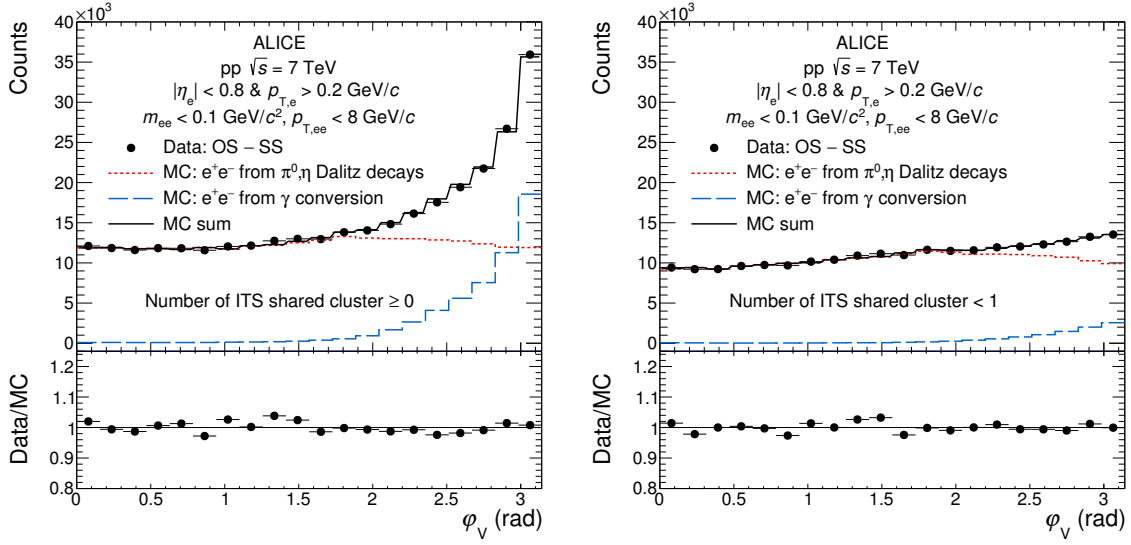
Figure 4. Measured φ_{v} distribution of correlated $\mathrm{e^+e^-}$ pairs with $m_{\mathrm{ee}} < 0.1\,\mathrm{GeV}/c^2$ and $p_{\mathrm{T,ee}} < 8\,\mathrm{GeV}/c$ compared with a sum of MC templates for different dielectron sources. The distributions are shown for all tracks including those that share some ITS clusters with other tracks (left) and with such tracks removed (right), as in the analysis. Only statistical uncertainties are shown for the data points.
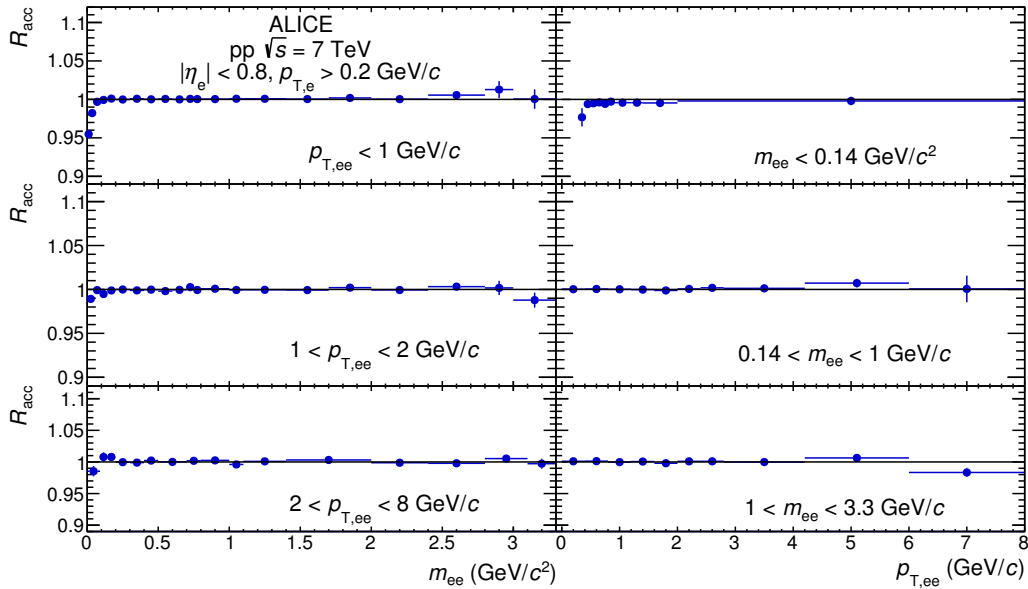

Figure 5. Relative acceptance correction factor R_{acc} as a function of m_{ee} (left) and $p_{\mathrm{T,ee}}$ (right). Statistical uncertainties are represented by vertical bars.
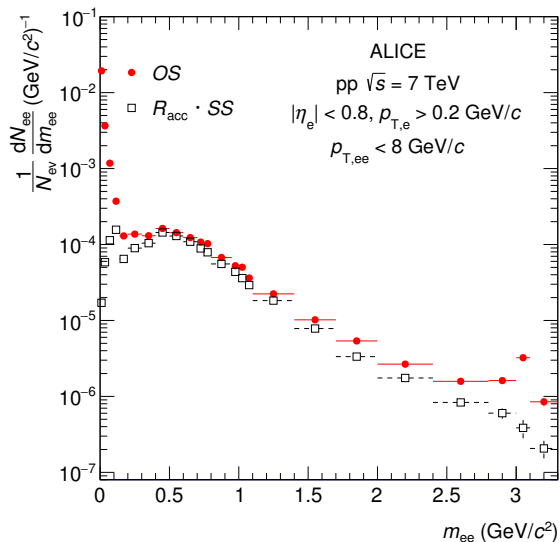
Figure 6. Opposite-sign m_{ee}-differential yield integrated in $p_{T,ee}$ and DCA$_{ee}$ overlaid with the same-sign spectrum corrected by the acceptance correction factor R_{acc}. Statistical uncertainties are represented by vertical bars.

malfunctioning detector segments and can be estimated by event mixing. The relative acceptance correction factor $R_{acc} = M_{+-}/(2 \cdot \sqrt{M_{++}M_{--}})$ is calculated, where M_{+-} and $M_{\pm\pm}$ are the mixed-event opposite-sign and same-sign pair distributions. The relative acceptance correction factor R_{acc} as a function of m_{ee} and $p_{T,ee}$ is shown in figure 5. For $\sqrt{(m_{ee}c)^2 + p_{T,ee}^2} > 1\,\text{GeV}/c$, R_{acc} is consistent with unity and no correction is applied, while at smaller m_{ee} and $p_{T,ee}$ deviations of up to 5% are observed. The relative acceptance correction factor is applied differentially in m_{ee}, $p_{T,ee}$, and DCA$_{ee}$.

In figure 6, the opposite-sign and relative-acceptance corrected same-sign m_{ee} spectra, i.e. OS and $R_{acc} \cdot SS$, are shown integrated over $p_{T,ee}$ and DCA$_{ee}$. The raw pair signal S is obtained with the formula:

$$S = OS - R_{acc} \cdot SS. \tag{3.7}$$

3.3 Efficiency corrections

The single-electron and pair efficiencies, including all tracking and PID selection criteria, are calculated using a detailed MC simulation. The event generator PYTHIA 6.4.25 [54] with the Perugia 2011 tune [67] is used to generate pp events. A realistic detector response is modelled using GEANT3 [68], with the same detector configurations as in data. The reconstruction efficiency (ϵ_e) for single-electron tracks does not show any dependence on the electron DCA, for which loose selection criteria were applied (DCA$_{xy} < 1$ cm and DCA$_z$ < 3 cm). Also no strong η dependence of ϵ_e is observed within $|\eta| < 0.8$ as well, whereas the dead zones of the first ITS layer can be seen in the φ distribution of the electron candidates due to the requirement of a hit in the first pixel. The random rejection probability of the prefilter algorithm is estimated by embedding test particles in real data events. It is found to be about 3% independent of p_T. The resulting pair efficiency $\epsilon_{rec}^{ee}(m_{ee}, p_{T,ee})$, shown
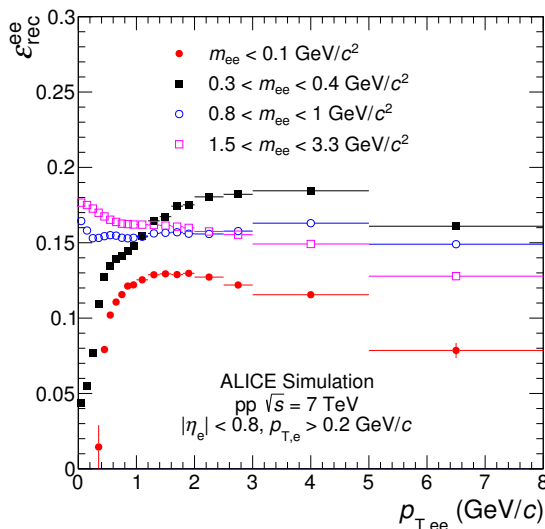
Figure 7. Pair efficiency as a function of $p_{\mathrm{T,ee}}$ for different m_{ee} intervals for the default electron selection criteria.

in a few selected intervals of m_{ee} in figure 7, is calculated and applied to the data as a function of m_{ee} and $p_{\mathrm{T,ee}}$. The efficiency of the φ_{v} requirement for dielectron pairs with $m_{\mathrm{ee}} < 0.1\,\mathrm{GeV}/c^2$ is estimated assuming that the φ_{v} distribution of the signal dielectron pairs is flat (see figure 4). For $m_{\mathrm{ee}} > 0.8\,\mathrm{GeV}/c^2$, $\epsilon^{\mathrm{ee}}_{\mathrm{rec}}(m_{\mathrm{ee}}, p_{\mathrm{T,ee}})$ reaches about 15%. At lower m_{ee}, the pair efficiency drops at low $p_{\mathrm{T,ee}}$.

Electrons suffer from Bremsstrahlung in the detector material, for which no correction is applied during the tracking procedure. This results in a smaller reconstructed momentum and distorts the shape of the m_{ee} distributions, which develop tails towards lower m_{ee}. Moreover, the reconstructed momentum of the electrons is also affected by the finite detector resolution. Such effects, i.e. p_{T}, θ, and φ single-track resolution and Bremsstrahlung, are not accounted for by the efficiency corrections, which do not contain any unfolding procedure. However, the detector reponses are folded into the particle spectrum generated by the hadronic cocktail, as explained in detail in [69].

The corrected number of dielectron pairs is expressed as:

$$\frac{\mathrm{d}^3 N_{\mathrm{e^+e^-}}}{\mathrm{d}m_{\mathrm{ee}}\,\mathrm{d}p_{\mathrm{T,ee}}\,\mathrm{d}\mathrm{DCA}_{\mathrm{ee}}} = \frac{1}{\Delta p_{\mathrm{T,ee}}}\frac{1}{\Delta m_{\mathrm{ee}}}\frac{1}{\Delta\mathrm{DCA}_{\mathrm{ee}}}\frac{S(m_{\mathrm{ee}}, p_{\mathrm{T,ee}}, \mathrm{DCA}_{\mathrm{ee}})}{\epsilon^{\mathrm{ee}}_{\mathrm{rec}}(m_{\mathrm{ee}}, p_{\mathrm{T,ee}})}, \qquad (3.8)$$

where $\Delta p_{\mathrm{T,ee}}$, Δm_{ee}, and $\Delta\mathrm{DCA}_{\mathrm{ee}}$ are the width of the $p_{\mathrm{T,ee}}$, m_{ee}, and $\mathrm{DCA}_{\mathrm{ee}}$ intervals, respectively. The spectra are finally normalised by the number of minimum bias pp collisions corrected for the primary vertex reconstruction efficiency, which is about 88%. The invariant dielectron cross section is obtained by multiplying the yield by the minimum bias pp cross section at $\sqrt{s} = 7\,\mathrm{TeV}$, of $\sigma_{\mathrm{MB}} = 62.4 \pm 2.2\,\mathrm{mb}$, which is estimated from the cross section σ_{V0AND} of the coincidence V0AND between signals in the two VZERO detectors, measured in a van der Meer scan [64]. The relative factor $\sigma_{\mathrm{V0AND}}/\sigma_{\mathrm{MB}}$ is given by the fraction of MB events where the L0 trigger input corresponding to the V0AND condition

Requirements	Variations
Hits required in the SPD	**in the first layer**, in both layers
Minimum number of ITS clusters	4, **5**, 6
Maximum χ^2 per ITS cluster	**4.5**, 3.5, 2.5
Maximum number of ITS shared clusters	**0**, 1, 2, 3, 4, 6
Minimum number of TPC clusters	80, **100**, 120
Minimum number of crossed rows in TPC	80, **100**, 130
Minimum ratio of crossed pad-rows to findable TPC clusters	0.5, **0.7**, 0.9
Maximum χ^2 per TPC cluster	**4**, 3, 2.5
TOF electron identification	$\lvert n_{\sigma_e}^{\mathrm{TOF}} \rvert < 2, \mathbf{3}, 4$
TPC electron identification	$\mathbf{-1.5}, -1, -0.5 < n_{\sigma_e}^{\mathrm{TPC}} < 2, 3, \mathbf{4}$
TPC pion rejection	$n_{\sigma_\pi}^{\mathrm{TPC}} < 3, \mathbf{3.5}, 4$
ITS electron identification	$-4, -3.5, \mathbf{-3} < n_{\sigma_e}^{\mathrm{ITS}} < 0, 0.5, \mathbf{1}$

Table 1. Summary of the single-track selection criterion variations to determine the systematic uncertainties. The default values are shown in bold.

has fired. Its value is 0.87, and is stable within 0.5% over the analyzed data sample. The corresponding normalisation uncertainty is $\pm 3.5\%$.

3.4 Systematic uncertainties

The systematic uncertainties arise from limitations in the determination of the background, the relative acceptance correction factor R_{acc}, the electron selection efficiency, the prefilter efficiency, and the pair-cut efficiency. These uncertainties are evaluated by varying all the electron and pair selection criteria simultaneously and by comparing the results with and without prefilter. Table 1 summarises the single-track selection criteria variations. The signal is extracted and corrected for 22 random combinations of selection criteria, which probe different but still reasonable single-electron efficiencies and S/B ratios, ranging from 0.22 to 0.42 at $p_{\mathrm{T}} = 1\,\mathrm{GeV}/c$ and from about 0.05 to 0.15 at $m_{\mathrm{ee}} = 0.5\,\mathrm{GeV}/c^2$, respectively. More than one selection criteria are varied at the same time to take into account possible correlations between them. The final systematic uncertainty is calculated as the root mean square of the variation of the final data points. These extracted systematic uncertainties contain not only systematic effects from the signal efficiency, but also from the background estimation. The maximum φ_{v} requirement for pairs with $m_{\mathrm{ee}} < 0.1\,\mathrm{GeV}/c^2$ is also varied, around the default value of 2 rad, from 1.57 to 2.5 rad. Deviations from a flat φ_{v} distribution for the signal dielectron pairs are estimated with a MC simulation and found to lead to a systematic uncertainty below 1% for the default φ_{v} requirement. The resulting systematic uncertainties from the selection criterion variation is listed in table 2 in the case of the DCA analysis with $p_{\mathrm{T,e}} > 0.4\,\mathrm{GeV}/c$.

An additional source of systematic uncertainty is considered for the $\mathrm{DCA}_{\mathrm{ee}}$-differential dielectron cross section. The electron efficiency is found to be independent on the single-track DCA within the range under study by checking the fraction of reconstructed electrons

Mass region	Uncertainty from DCA$_{ee}$-$p_{T,ee}$ correlation	Uncertainty from selection criterion variation
$m_{ee} < 0.14\,\mathrm{GeV}/c^2$	–	8.7%
$0.14 < m_{ee} < 1.1\,\mathrm{GeV}/c^2$	1.5%	11%
$1.1 < m_{ee} < 2.7\,\mathrm{GeV}/c^2$	3.0%	17%
$2.7 < m_{ee} < 3.3\,\mathrm{GeV}/c^2$	4.9%	17%

Table 2. Summary of the systematic uncertainties for the DCA$_{ee}$ analysis ($p_{T,e} > 0.4\,\mathrm{GeV}/c$ and $|\eta_e| < 0.8$).

as a function of the distance of their production vertex to the reconstructed primary vertex in MC. However, some correlations still remain between $p_{T,ee}$ and DCA$_{ee}$. In the π^0 mass region ($0.08 < m_{ee} < 0.14\,\mathrm{GeV}/c^2$), the mean $p_{T,ee}$ is approximately constant as a function of DCA$_{ee}$, which is expected since the electron tracks should always point to the primary vertex for a prompt source, and the finite DCA$_{ee}$ values are only due to the detector resolution. This is not the case for the J/ψ region ($2.7 < m_{ee} < 3.3\,\mathrm{GeV}/c^2$), where the mean $p_{T,ee}$ exhibits an increase as a function of DCA$_{ee}$. The reasons are twofold: first, non-prompt J/ψ from feed-down from B-mesons have a harder p_T spectrum than prompt J/ψ, and second, high-p_T non-prompt J/ψ decay farther away than low-p_T non-prompt J/ψ so that the decay electrons have larger DCAs and larger p_T compared to electrons from low-p_T non-prompt J/ψ. The possible remaining uncertainty from this correlation is estimated by half the difference of the pair efficiency at the maximum and minimum mean-$p_{T,ee}$, seen as a function of DCA$_{ee}$ in a given mass region. This systematic uncertainty is found to be less than 5%, increasing from low to high m_{ee}. Table 2 summarises the systematic uncertainties arising from the DCA analysis.

4   Cocktail of hadronic sources

To allow for a detailed interpretation of the data, the contribution from all known hadronic sources must be estimated. The so-called hadronic cocktail contains contributions from pseudoscalar and vector-meson decays as well as from semileptonic decays of heavy-flavour hadrons.

4.1   e$^+$e$^-$ pairs from light-flavour hadrons and J/ψ mesons

The Dalitz decays of light neutral mesons, $\pi^0 \to \mathrm{e^+e^-}\,\gamma$, $\eta \to \mathrm{e^+e^-}\,\gamma$, $\eta' \to \mathrm{e^+e^-}\,\gamma$, $\eta' \to \mathrm{e^+e^-}\,\omega$, $\omega \to \mathrm{e^+e^-}\,\pi^0$, $\phi \to \mathrm{e^+e^-}\,\eta$, and $\phi \to \mathrm{e^+e^-}\,\pi^0$, and the dielectron decays of the vector mesons, ρ, ω, ϕ, and J/ψ are simulated with the phenomenological event generator EXODUS [23]. The radiative decay of J/ψ ($J/\psi \to \mathrm{e^+e^-}\,\gamma$) is also included. The pair mass distribution from the Dalitz decays follows the Kroll-Wada expression [70] multiplied by the electromagnetic form factors measured by the Lepton-G Collaboration [71, 72] and more recently by the NA60 Collaboration [73, 74]. The ρ line shape has been studied in detail in p$-$A collisions at $400\,\mathrm{GeV}$ by the NA60 Collaboration [73], who confirmed the

need for a Boltzmann term beyond the standard description [75] and provided a precise measurement of the effective temperature parameter. For the decay of the other vector mesons, which are assumed to be unpolarised, the Gounaris-Sakurai expression [76] is used.

The rapidity distribution of the mesons is assumed to be flat at mid-rapidity. The momentum distributions of π^0, η, ϕ, and J/ψ are obtained by fitting the spectra measured by the ALICE Collaboration [77–80] with a modified Hagedorn function [81]. The measured $\pi^\pm$ and π^0 spectra agree within their systematic uncertainties. Since the $\pi^\pm$ measurement extends to lower p_T, and exhibits smaller uncertainties than the π^0, charged pions are used to approximate neutral pions. For the other mesons, ρ, ω, and η', the shape of their p_T spectra is derived from the $\pi^\pm$ spectrum. The η' mesons are generated assuming m_T scaling [82–84], implying that the spectra of all light mesons as a function of $m_T = \sqrt{m^2 + p_T^2}$ are the same and only differ by a normalisation factor. The normalisation factors are based on the ratio of the p_T spectra of the given hadron to the p_T spectrum of the $\pi^\pm$ at high p_T: 0.4 ± 0.08 for η' from PYTHIA 6 calculations of pp collisions at $\sqrt{s} = 7\,\mathrm{TeV}$, 0.85 ± 0.17 for ω obtained from measurements in pp collisions at $\sqrt{s} = 7\,\mathrm{TeV}$ [85], and 1.0 ± 0.2 for ρ obtained from measurements in pp collisions at $\sqrt{s} = 2.76\,\mathrm{TeV}$ [86]. The momentum distributions of ω and ρ are obtained from the $\omega/\pi^\pm$ and $\rho/\pi^\pm$ ratios in simulated pp collisions at $\sqrt{s} = 7\,\mathrm{TeV}$ with the Monash 2013 tune of PYTHIA 8 [87, 88]. This tune describes the measured ω/π^0 and ρ/π^0 ratios in pp collisions at $\sqrt{s} = 7\,\mathrm{TeV}$ and $2.76\,\mathrm{TeV}$, respectively. Since the ω measurement does not extend to low p_T (the ω meson is measured for $p_T > 2\,\mathrm{GeV}/c$), fits of the data are used only to estimate the systematic uncertainties.

The expected dielectron yield as a function of m_{ee} and $p_{T,ee}$ is computed in a fast simulation by filtering the generated hadronic cocktail through the ALICE acceptance, while applying the detector responses including the momentum and opening angle resolutions, and the Bremsstrahlung effect [69], since no unfolding procedure is applied to the data. The momentum transformation matrices are determined with full GEANT3 [68] simulations of the interactions of the primary electrons produced in pp collisions with the material of the ALICE apparatus.

The main systematic uncertainties on the hadronic cocktail arise from the uncertainties of the measured $\pi^\pm$, η, ω, ϕ, and J/ψ p_T spectra and those of the m_T normalisation factors. The first is evaluated by parameterising the data along the upper and lower ends of their statistical and systematic uncertainties added in quadrature. The complete cocktail of e^+e^- pairs is then generated again based on these new parametrisations. For the ρ mesons, m_T scaling is used to estimate the systematic uncertainties originating from the ρ p_T spectrum. The uncertainties from the different decay branching ratios [89] are also taken into account.

4.2 Open-charm and open-beauty contributions to the dielectron yield

Electron pairs that originate from the semileptonic decays of $c\bar{c}$ and $b\bar{b}$ are simulated with two different generators, the leading-order (LO) event generator PYTHIA 6.4.25 [54], and the next-to-leading order (NLO) event generator POWHEG [55, 56]. The $c\bar{c}$ and $b\bar{b}$ pairs are produced at leading order through pair creation, predominantly $gg \to Q\overline{Q}$ with a small contribution of $q\bar{q} \to Q\overline{Q}$, where g, q, and Q are gluons, up or down quarks, and charm or

beauty quarks, respectively. At higher order, flavour excitations and gluon splitting give rise to further contributions.

PYTHIA simulations utilise LO-pQCD matrix elements for $2 \to 2$ processes together with a leading-logarithmic p_T-ordered parton shower, and an underlying-event simulation including multiple parton interactions. The fragmentation and hadronisation of the charm and beauty quarks are based on the Lund string model. In this paper, the Perugia-2011 tune [67] is used, for which the first LHC data, mainly from multiplicity and underlying-event related measurements, have been considered. In this tune, the parton distribution functions are parametrised with the CTEQ5L [90] functions.

POWHEG is a NLO-pQCD generator that can be interfaced to a parton shower MC (e.g. from PYTHIA or HERWIG [91]) to provide final-state particles. The calculations presented in this paper (POWHEG) are obtained with the POWHEG BOX framework [57, 58] and the tune Perugia-2011 of PYTHIA 6.4.25. The CTEQ6.6 [92] functions are used for the input parton distribution functions. To be consistent with the PYTHIA simulations, the mass of the charm and beauty quarks are set to $1.5\,\mathrm{GeV}/c^2$ and $4.75\,\mathrm{GeV}/c^2$, respectively.

The simulations are normalised to the measured total charm and beauty cross section, i.e. $\sigma_{c\bar{c}}^{\mathrm{REF}} = 7.44 \pm 0.14(\text{stat.}) \pm 0.58(\text{syst.})\,\mathrm{mb}$ [93] and $\sigma_{b\bar{b}}^{\mathrm{REF}} = 288 \pm 4(\text{stat.}) \pm 48(\text{syst.})\,\mu\mathrm{b}$ [94] and passed through the ALICE acceptance after applying the detector responses including the momentum and opening angle resolutions, and the Bremsstrahlung effect [69]. The systematic uncertainties of the $\sigma_{c\bar{c}}^{\mathrm{REF}}$ and $\sigma_{b\bar{b}}^{\mathrm{REF}}$ measurements are propagated to the final hadronic cocktail. Whereas the effective beauty-to-electron branching ratio is taken from PYTHIA ($\mathrm{BR}_{b(\to c)\to e} = \mathrm{BR}_{b\to c\to e} + \mathrm{BR}_{b\to e} = 11.7 + 10.2 = 21.9\%$ consistent with [89]), the one for charm-to-electron ($\mathrm{BR}_{c\to e}$) is assumed to be $(9.6 \pm 0.4)\%$ as reported in [89], which is slightly smaller than what has been estimated with PYTHIA ($\mathrm{BR}_{c\to e} = 10.6\%$). An additional uncertainty of 9.3% is added in quadrature for the $\mathrm{BR}_{c\to e}$ to take into account differences in the Λ_c^+/D^0 ratio measured by the ALICE Collaboration, $0.543\pm0.061(\text{stat.})\pm0.160(\text{syst.})$ (for $p_T > 1\,\mathrm{GeV}/c$) in pp collisions at $\sqrt{s} = 7\,\mathrm{TeV}$ [95], and the LEP average of $0.113 \pm 0.013(\text{stat.}) \pm 0.006(\text{syst.})$ [96]. This translates into a 22% uncertainty at the pair level. The uncertainties of the effective beauty- and charm-to-electron branching ratios are propagated to the final hadronic cocktail. For both generators, the p_T-differential cross-section of single electrons from charm- and beauty-hadron decays at mid-rapidity is found to be consistent with FONLL calculations [97] and to reproduce the measurements reasonably well within the theoretical and experimental uncertainties [98]. To obtain the dielectron yield of correlated $\mathrm{e}^+\mathrm{e}^-$ pairs from heavy-flavour hadron decays, the distribution of same-sign pairs is subtracted from the $\mathrm{e}^+\mathrm{e}^-$ spectrum, as in data.

4.3 DCA$_{ee}$ template distributions

Whereas the differential $p_{T,ee}$ and m_{ee} distributions of the hadronic cocktail are estimated from a fast simulation, the DCA$_{ee}$ distributions are determined with a full GEANT3 [68] simulation of the ALICE detector. For this purpose, PYTHIA 6.4.25 events are passed through the full detector simulation tuned to describe the performance of each detector subsystem. In particular, all relevant charactereristics of the SPD, such as a map of dead channels, are included in the simulation. The same analysis selection criteria as in data are
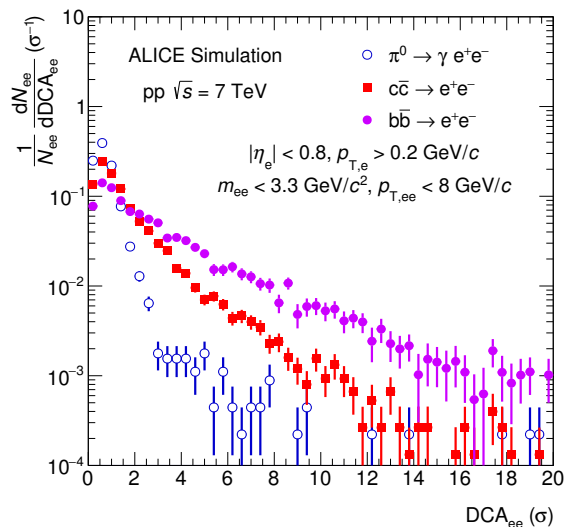
Figure 8. DCA$_{ee}$ distributions of e$^+$e$^-$ pairs from π^0 Dalitz decays, from semileptonic decays of charm and beauty hadrons in MC simulations (see text), integrated over m_{ee} and $p_{T,ee}$.

applied. Since the various charm hadrons have quite different decay lengths, ranging from about $59.9\,\mu$m for $\Lambda_c^\pm$ to $311.8\,\mu$m for D$^\pm$ mesons [89], their relative yields are relevant to build the DCA$_{ee}$ template of correlated e$^+$e$^-$ pairs from charm-hadron decays. The measured production ratios of charm hadrons [95, 99] and their semileptonic decay branching ratios [89] are used to obtain the c$\bar{c}$ DCA$_{ee}$ distribution. Finally, DCA$_{ee}$ templates are extracted for e$^+$e$^-$ pairs from π^0 Dalitz decays, from charm- and beauty-hadron decays, and from the decays of prompt and non-prompt J/ψ. In figure 8, the π^0, c$\bar{c}$, and b$\bar{b}$ templates are shown integrated over $p_{T,ee}$ and m_{ee}. Whereas the distributions for prompt sources, like π^0, directly reflect the detector DCA resolution, those of non-prompt sources, like heavy-flavour hadrons, are characterised by the convolution of the DCA resolution and the decay length of the mother particle ($c\tau_D \approx 150\,\mu$m and $c\tau_B \approx 470\,\mu$m [89]). The DCA$_{ee}$ spectrum of e$^+$e$^-$ pairs from π^0 Dalitz decays is taken as an approximation for all prompt light-flavour decays into dielectrons.

Each contribution is normalised to its expected yield from the hadronic cocktail in the same m_{ee} and $p_{T,ee}$ range and after the same fiducial selection criteria ($|\eta_e| < 0.8$ and $p_{T,e} > 0.4\,\text{GeV}/c$). Since e$^+e^-$ pairs from prompt and non-prompt J/ψ have different DCA$_{ee}$ distributions, the measured fraction of non-prompt J/ψ in pp collisions at 7 TeV [100], f_B, is used to scale the templates accordingly. To evaluate the uncertainty originating from f_B, the DCA$_{ee}$ distributions are shifted to the upper and lower bounds of the statistical and systematic uncertainties added in quadrature.

Additional sources of systematic uncertainties are considered. First, the resolution of the single-track DCA is found to be better in MC as compared to data by about 15%. This affects the DCA$_{ee}$ distributions, in particular those of e$^+$e$^-$ pairs from prompt sources like π^0 and prompt J/ψ, at around 1-3 σ. Second, the uncertainties on the charm-hadron production ratios [95, 99] and on their semileptonic decay branching ratios [89] are propa-

gated to the final DCA_{ee} distribution of correlated e^+e^- pairs from charm-hadron decays. Third, the PYTHIA simulations used to create the DCA_{ee} templates for the heavy-flavour contributions have been performed with the PYTHIA Perugia-0 tune [67], which does not reproduce well the measured p_T distribution of electrons from charm-hadron decays at high p_T ($p_T > 3\,\text{GeV}/c$) [98]. This was found to have a negligible effect on the final DCA_{ee} template, by varying the maximum p_T requirement on the single electron track ($p_T < 3\,\text{GeV}/c$). Moreover, the charm and beauty DCA_{ee} templates do not exhibit any strong dependence on $p_{T,ee}$ and m_{ee}, as well as on the minimum electron p_T requirement. The latter is varied from $0.4\,\text{GeV}/c$ to $0.7\,\text{GeV}/c$. Therefore, the shape of the heavy-flavour MC templates is assumed to be model independent, whereas their absolute normalisation, i.e. the dielectron yields from charm- and beauty-hadron decays in the given $p_{T,ee}$ and m_{ee} range, is not. The same DCA_{ee} distributions are used for the two event generators, PYTHIA and POWHEG, and normalised to the dielectron yield predicted in each mass interval by the corresponding event generator.

5 Results and discussion

5.1 Comparison of the data to the cocktail

The differential e^+e^- cross section $d\sigma/dm_{ee}$ in minimum bias pp collisions at $\sqrt{s} = 7\,\text{TeV}$ is presented in figure 9 in the ALICE acceptance ($|\eta_e| < 0.8$ and $p_{T,e} > 0.2\,\text{GeV}/c$) as a function of m_{ee}. Statistical and systematic uncertainties of the data are indicated by vertical bars and boxes, respectively. The measured spectrum is compared with the cocktail of expected e^+e^- sources, where PYTHIA is used to calculate the correlated pairs from heavy-flavour decays. The total systematic uncertainty of the cocktail is shown by the grey band. The bottom panel shows the ratio of data to cocktail. Good agreement is observed over the full mass range ($m_{ee} < 3.3\,\text{GeV}/c^2$).

For a more detailed discussion, the results are presented differentially below in $p_{T,ee}$ and DCA_{ee} in four different mass regions, i.e. the π^0 region ($m_{ee} < 0.14\,\text{GeV}/c^2$), the low-mass region ($0.14 < m_{ee} < 1.1\,\text{GeV}/c^2$), the IMR ($1.1 < m_{ee} < 2.7\,\text{GeV}/c^2$), and the J/ψ region ($2.7 < m_{ee} < 3.3\,\text{GeV}/c^2$).

5.1.1 π^0 mass region

The mass region $m_{ee} < 0.14\,\text{GeV}/c^2$ is dominated by π^0 Dalitz decays ($\pi^0 \to e^+e^-\gamma$), with a small contribution from η Dalitz decays ($\eta \to e^+e^-\gamma$) of about 10%. In the left panel of figure 10, the measured $p_{T,ee}$-differential cross section of e^+e^- pairs is shown in comparison with the hadronic cocktail. Good agreement between data and cocktail is observed within the systematic uncertainties. This confirms that the dielectron analysis is consistent with the previous light-meson measurements [77–79, 85] taken as input for the calculations of the expected e^+e^- cross section.

In the right panel of figure 10, the measured e^+e^- cross section is shown as a function of DCA_{ee} in the mass range $0.08 < m_{ee} < 0.14\,\text{GeV}/c^2$ for $p_{T,ee} < 8\,\text{GeV}/c$. The results are compared with the expectations from MC. The low-mass cut-off at $0.08\,\text{GeV}/c^2$ is chosen such that residual contaminations of e^+e^- pairs from photon conversions with large
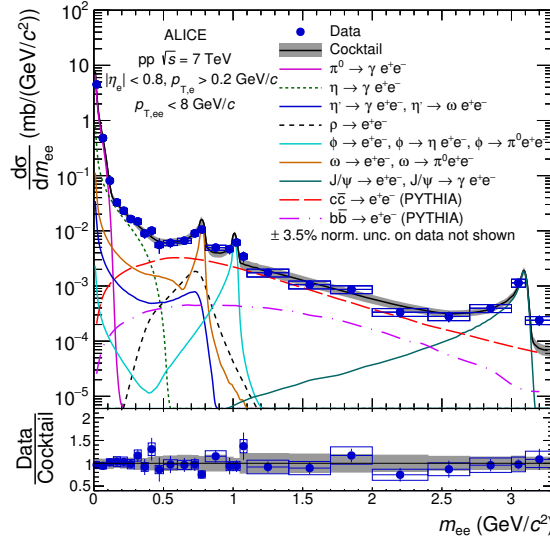
Figure 9. (Colour online) Inclusive e^+e^- cross section in pp collisions at $\sqrt{s} = 7\,\text{TeV}$ in the ALICE acceptance as a function of mass. The data are compared with a cocktail of expected sources. In the lower panel, the ratio of data to cocktail is shown. Statistical and systematic uncertainties of the data are plotted as vertical bars and boxes, respectively. The total uncertainty of the cocktail is represented as a grey band.
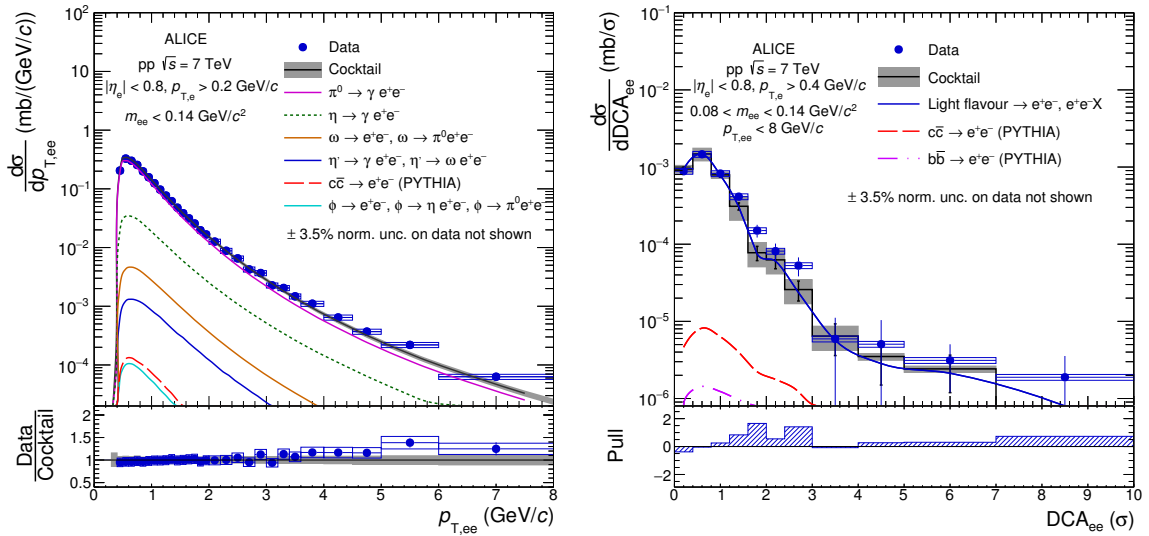

Figure 10. (Colour online) Inclusive e^+e^- cross section in pp collisions at $\sqrt{s} = 7\,\text{TeV}$ in the ALICE acceptance as a function of $p_{\text{T,ee}}$ (left) and DCA_{ee} (right) for $m_{\text{ee}} < 0.14\ \text{GeV}/c^2$ and $0.08 < m_{\text{ee}} < 0.14\ \text{GeV}/c^2$, respectively. The data are compared with a cocktail of expected sources. In the bottom panels, the ratio of data to cocktail as a function of $p_{\text{T,ee}}$ (left) and the pull distribution as a function of DCA_{ee} (right) are shown. Statistical and systematic uncertainties on the data are plotted as vertical bars and boxes, respectively. The total uncertainty of the cocktail is represented as a grey band.

– 19 –

DCA$_\text{ee}$ values are suppressed. The blue line represents the expected cross section of all prompt light-flavour sources, for which the π^0 DCA$_\text{ee}$ template is used as an approximation. Some small statistical fluctuations can be seen in the tail of the distribution, which would require a very large amount of fully simulated pp collisions to be removed. In this mass range, the contributions from non-prompt sources ($c\bar{c}$ and $b\bar{b}$) are negligible, which allows the DCA$_\text{ee}$ resolution in data and in MC to be directly compared. To quantify the agreement between data and the expected DCA$_\text{ee}$ distribution from MC, the pull distribution is shown in the bottom right panel of figure 10. It is defined as the difference between data and MC normalised by the quadratic sum of their statistical and systematic uncertainties. The DCA$_\text{ee}$ distribution obtained from the full simulations of the ALICE detector describes the data well. A slight excess of the data is observed in $1 < \text{DCA}_\text{ee} < 3\,\sigma$ which is the range mostly affected by discrepancies in the DCA resolution between data and MC.

5.1.2 Low-mass region

The low-mass region, $0.14 < m_\text{ee} < 1.1\,\text{GeV}/c^2$, is expected to be dominated by the light mesons η, $\eta^{'}$, ρ, ω, ϕ, and the contribution of correlated e$^+$e$^-$ pairs from semileptonic decays of charm hadrons. A very small contribution of virtual direct photons is also expected (3–5% of the total measured yield in $0.14 < m_\text{ee} < 0.7\,\text{GeV}/c^2$ and $4 < p_\text{T,ee} < 8\,\text{GeV}/c$). The latter is not included in the hadronic cocktail and will be discussed in section 5.2. At low m_ee ($m_\text{ee} \leq m_\eta$), the η Dalitz decay is the main source of e$^+$e$^-$ pairs for all $p_\text{T,ee}$, as shown in the left panel of figure 11, whereas at larger m_ee, the heavy-flavour contributions start to dominate, followed by the ω, ρ, and ϕ contributions (see right panel of figure 11). The requirement on the single electron track of $p_\text{T} > 0.2\,\text{GeV}/c$ produces an acceptance hole at low m_ee and $p_\text{T,ee}$, which can be seen in the data in the m_ee interval $0.14 < m_\text{ee} < 0.7\,\text{GeV}/c^2$ for the $p_\text{T,ee}$ range $0 < p_\text{T,ee} < 0.4\,\text{GeV}/c$ (see left panel of figure 11). Due to their characteristic m_ee and $p_\text{T,ee}$ distributions, the e$^+$e$^-$ pairs of the various expected sources are differently affected. The hadronic cocktail is well in agreement with the data within the statistical and systematic uncertainties.

The mixture of prompt and non-prompt sources in the low-mass region makes it well suited to test the feasibility to separate prompt and non-prompt contributions via the DCA$_\text{ee}$ variable. In figure 12, the DCA$_\text{ee}$-differential cross section of e$^+$e$^-$ pairs is shown integrated over $p_\text{T,ee}$ in the mass range $0.14 < m_\text{ee} < 1.1\,\text{GeV}/c^2$. The template for e$^+e^-$ pairs from prompt light-flavour hadron decays cannot describe the tail of the DCA$_\text{ee}$ distribution. The latter is well reproduced by additional contributions from correlated pairs of heavy-flavour hadron decays. The good agreement between data and MC validates the possibility to separate prompt from non-prompt dielectron sources via this observable.

5.1.3 Intermediate-mass region

The IMR, $1.1 < m_\text{ee} < 2.7\,\text{GeV}/c^2$, is dominated by correlated e$^+$e$^-$ pairs from semileptonic decays of charm and beauty hadrons. The $p_\text{T,ee}$-differential cross section of e$^+$e$^-$ pairs measured in this m_ee region is shown in comparison with the hadronic cocktail in the left panel of figure 13. The cross section of e$^+$e$^-$ pairs from $c\bar{c}$ is the dominant dielectron source
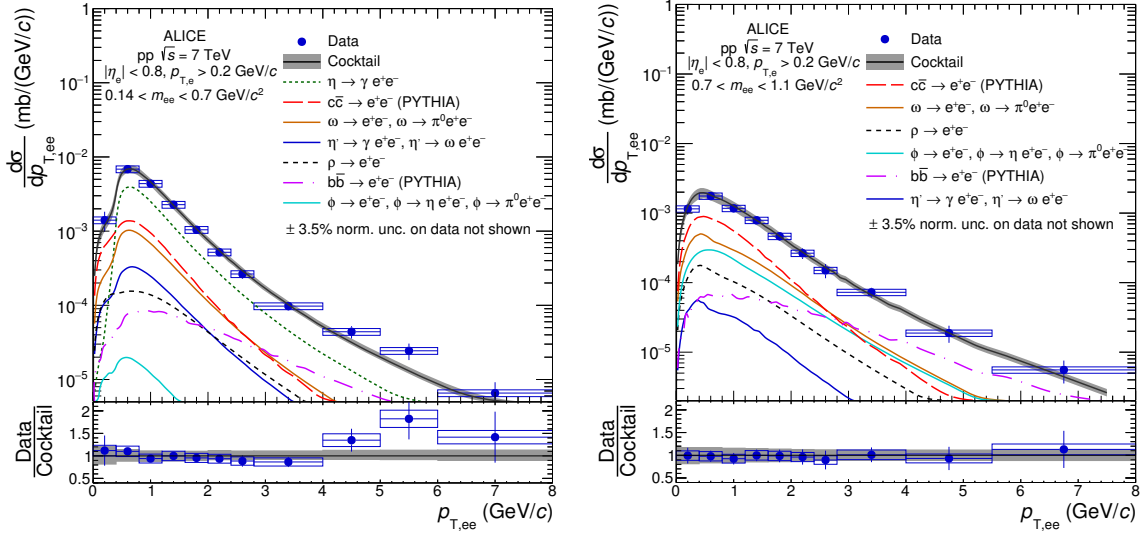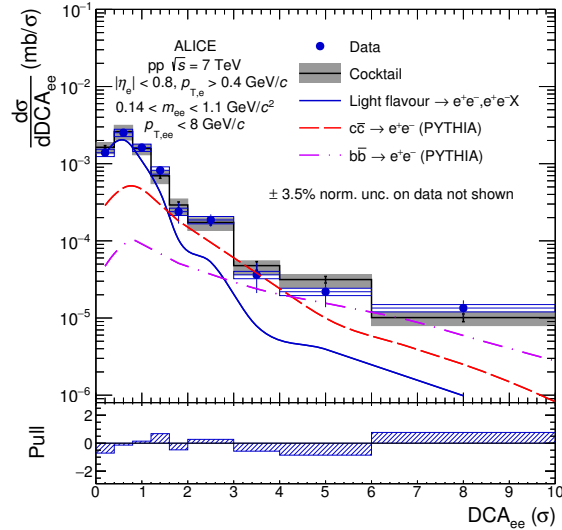
Figure 11. (Colour online) Inclusive e^+e^- cross section in pp collisions at $\sqrt{s} = 7\,\text{TeV}$ in the ALICE acceptance as a function of $p_{\text{T,ee}}$ in the mass range $0.14 < m_{ee} < 0.7\,\text{GeV}/c^2$ (left) and $0.7 < m_{ee} < 1.1\,\text{GeV}/c^2$ (right). The data are compared with the hadronic cocktail. In the bottom panels, the ratios of data to cocktail as a function of $p_{\text{T,ee}}$ are shown. Statistical and systematic uncertainties on the data are plotted as vertical bars and boxes, respectively. The total uncertainty of the cocktail is represented as a grey band.
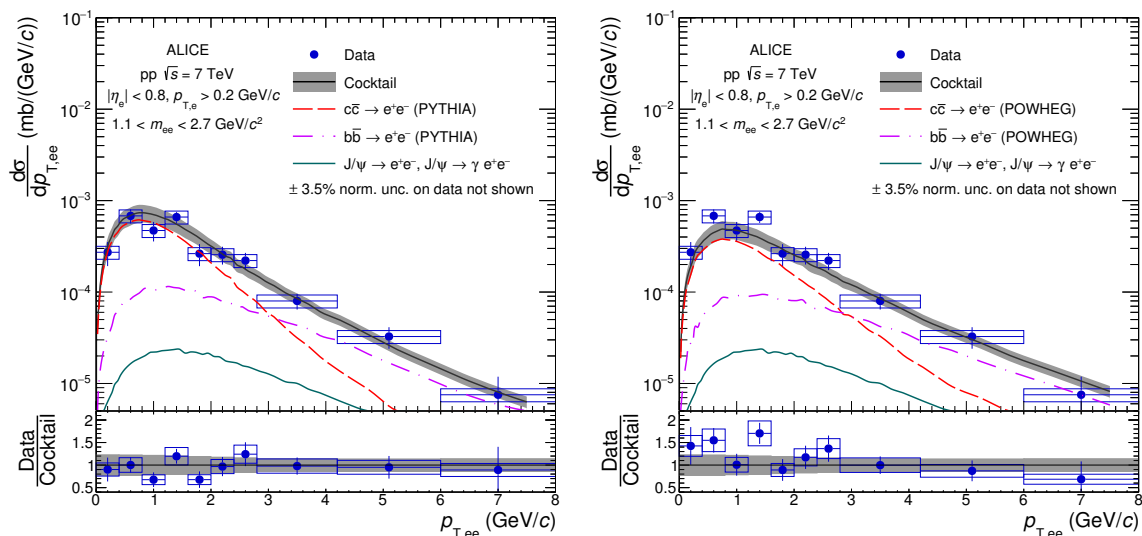

Figure 12. (Colour online) Inclusive e^+e^- cross section in pp collisions at $\sqrt{s} = 7\,\text{TeV}$ in the ALICE acceptance as a function of DCA_{ee} in the mass range $0.14 < m_{ee} < 1.1\,\text{GeV}/c^2$. The data are compared with a cocktail of expected sources. In the bottom panel, the pull distribution is shown. Statistical and systematic uncertainties on the data are plotted as vertical bars and boxes, respectively. The total uncertainty of the cocktail is represented as a grey band.

Figure 13. (Colour online) Inclusive e^+e^- cross section in pp collisions at $\sqrt{s} = 7\,\mathrm{TeV}$ in the ALICE acceptance as a function of $p_{T,ee}$ in the mass range $1.1 < m_{ee} < 2.7\,\mathrm{GeV}/c^2$. The data are compared with the hadronic cocktail, where PYTHIA [54] (left) and POWHEG [55–58] (right) are used to calculate the $c\bar{c}$ and $b\bar{b}$ contributions. In the bottom panels, the corresponding ratios of data to cocktail as a function of $p_{T,ee}$ are shown. Statistical and systematic uncertainties on the data are plotted as vertical bars and boxes, respectively. The total uncertainty of the cocktails is represented as a grey band.

for $p_{T,ee} < 3\,\mathrm{GeV}/c$, whereas most of the e^+e^- pairs originate from $b\bar{b}$ for $p_{T,ee} > 4\,\mathrm{GeV}/c$. This allows the correlated pairs from semileptonic decays of charm and beauty hadrons to be separated. Reasonable agreement between data and cocktail is seen in the bottom left panel of figure 13. The data are compared with a hadronic cocktail in the right panel of figure 13 where POWHEG is used to calculate the $c\bar{c}$ and $b\bar{b}$ contributions. The NLO event generator predicts harder $p_{T,ee}$ spectra for the $c\bar{c}$ and $b\bar{b}$ contributions. For the same global normalisation to $\sigma_{c\bar{c}}^{\mathrm{REF}}$ and $\sigma_{b\bar{b}}^{\mathrm{REF}}$ as for the PYTHIA cocktail, the POWHEG calculations tend to underestimate the data, in particular in the region where the $c\bar{c}$ contribution dominates. This indicates a sensitivity of the present data to the underlying heavy-quark production mechanism implemented in the two models. The latter can result in different kinematic correlations of the $Q\bar{Q}$ pair and therefore different probabilities for the e^+e^- pair to enter the detector acceptance.

Table 3 summarises the fraction of correlated e^+e^- pairs in the full phase space (4π) and after consecutive acceptance selection criteria for the $c\bar{c}$ and $b\bar{b}$ contributions. The fraction of dielectron pairs from charm-hadron decays where both electrons are found at mid-rapidity ($|\eta_{e^\pm}| < 0.8$) is about 5.2% and 7.5% for the POWHEG and PYTHIA simulation, respectively. Since the hadronisation of the charm and beauty quarks, as well as the decay kinematics of the heavy-flavour hadrons, are the same in both calculations, this difference results from different treatments of the various production processes of the $c\bar{c}$ pair by the two event generators. First, the rapidity distribution of charm quarks predicted by POWHEG is slighly broader than the one from PYTHIA, leading to a smaller probability for single electrons to fall into the acceptance at mid-rapidity in POWHEG (17.3%) as com-

c$\bar{\mathrm{c}}$	PYTHIA	POWHEG	PYTHIA/POWHEG
4π	1.	1.	
$|\eta_{\mathrm{e}}| < 0.8$ (uncorrelated e$^+$e$^-$)	0.0754 (0.0428)	0.0518 (0.0299)	1.46 (1.43)
$|\eta_{\mathrm{e}}| < 0.8$ $1.1 < m_{\mathrm{ee}} < 2.7\,\mathrm{GeV}/c^2$	0.0148	0.0100	1.48
$|\eta_{\mathrm{e}}| < 0.8$ & $p_{\mathrm{T,e}} > 0.2\,\mathrm{GeV}/c$ $1.1 < m_{\mathrm{ee}} < 2.7\,\mathrm{GeV}/c^2$	0.0146	0.0098	1.49
$|\eta_{\mathrm{e}}| < 0.8$ & $p_{\mathrm{T,e}} > 0.4\,\mathrm{GeV}/c$ $1.1 < m_{\mathrm{ee}} < 2.7\,\mathrm{GeV}/c^2$	0.0115	0.0077	1.49
b$\bar{\mathrm{b}}$	PYTHIA	POWHEG	PYTHIA/POWHEG
4π	1	1	
$|\eta_{\mathrm{e}}| < 0.8$ (uncorrelated e$^+$e$^-$)	0.1250 (0.0581)	0.1167 (0.0506)	1.07 (1.15)
$|\eta_{\mathrm{e}}| < 0.8$ $1.1 < m_{\mathrm{ee}} < 2.7\,\mathrm{GeV}/c^2$	0.0495	0.0472	1.05
$|\eta_{\mathrm{e}}| < 0.8$ & $p_{\mathrm{T,e}} > 0.2\,\mathrm{GeV}/c$ $1.1 < m_{\mathrm{ee}} < 2.7\,\mathrm{GeV}/c^2$	0.0484	0.0460	1.05
$|\eta_{\mathrm{e}}| < 0.8$ & $p_{\mathrm{T,e}} > 0.4\,\mathrm{GeV}/c$ $1.1 < m_{\mathrm{ee}} < 2.7\,\mathrm{GeV}/c^2$	0.0413	0.0390	1.06

Table 3. Fraction of correlated e$^+$e$^-$ pairs in 4π and after consecutive acceptance selection criteria (left column) for two different event generators (PYTHIA/POWHEG) and their relative difference (right column).

pared to PYTHIA (20.7%). Second, the pseudorapidity correlation between the electron and positron from charm-hadron decays gives rise to a larger acceptance for e$^+$e$^-$ pairs at mid-rapidity than from a purely random correlation. The pseudorapidity correlation is model-dependent which increases the difference in acceptance between the two generators to about 46%. For electrons from beauty-hadron decays, the model dependences are smaller, on the order of 7%. The rapidity distributions of beauty quarks predicted by POWHEG and PYTHIA are quite similar. Moreover, about 50% of the correlated e$^+$e$^-$ pairs from beauty hadron decays originate from a single B hadron (B $\rightarrow$ $\overline{\mathrm{D}}$e$^+$X $\rightarrow$ e$^+$e$^-$X) and are insensitive to the correlations between the B and $\overline{\mathrm{B}}$ hadrons. Due to the large mass of the B hadrons, the correlation between the decay electron and the parent meson is diluted and the pseudorapidity correlation of the e$^+$e$^-$ pairs originating from different B hadrons is less related to the correlation between the b and $\overline{\mathrm{b}}$ but more driven by decay kinematics.

The measured DCA$_{\mathrm{ee}}$ distribution of e$^+$e$^-$ pairs is shown in figure 14 integrated over $p_{\mathrm{T,ee}}$ in the mass range $1.1 < m_{\mathrm{ee}} < 2.7\,\mathrm{GeV}/c^2$. The results are compared with the MC
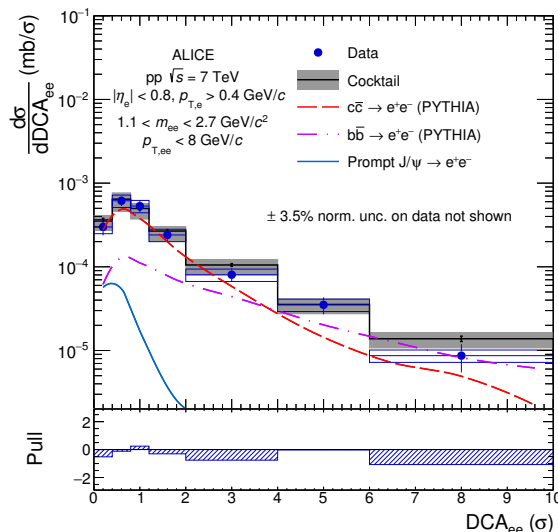
Figure 14. (Colour online) Inclusive e^+e^- cross section in pp collisions at $\sqrt{s} = 7\,\mathrm{TeV}$ in the ALICE acceptance as a function of $\mathrm{DCA_{ee}}$ in the mass range $1.1 < m_{ee} < 2.7\,\mathrm{GeV}/c^2$. The data are compared with a cocktail of expected sources. In the bottom panel, the pull distribution is shown. Statistical and systematic uncertainties on the data are plotted as vertical bars and boxes, respectively. The total uncertainty of the cocktail is represented as a grey band.

templates normalised to the PYTHIA cocktail. The shape of the MC $\mathrm{DCA_{ee}}$ distribution for correlated e^+e^- pairs from charm-hadron decays deviates from the data at large $\mathrm{DCA_{ee}}$. The additional contribution from e^+e^- pairs from beauty-hadron decays allows the data to be well described, as can be seen with the pull distribution presented in the bottom panel of figure 14. The $\mathrm{DCA_{ee}}$ variable gives additional constraints to separate e^+e^- pairs from charm- and beauty-hadron decays. No indication for a prompt source is observed in the IMR.

The total $c\bar{c}$ and $b\bar{b}$ cross sections, $\sigma_{c\bar{c}}$ and $\sigma_{b\bar{b}}$, can be extracted from the data by fitting the measured e^+e^- cross section of heavy-flavour hadron decays in the IMR with the sum of two contributions:

$$f^{\mathrm{GEN}} = S_{c\bar{c}}\,f^{\mathrm{GEN}}_{c\bar{c}} + S_{b\bar{b}}\,f^{\mathrm{GEN}}_{b\bar{b}}, \tag{5.1}$$

where $f^{\mathrm{GEN}}_{c\bar{c}}$ and $f^{\mathrm{GEN}}_{b\bar{b}}$ are the cross sections for dielectron pairs from charm and beauty-hadron decays, calculated with the event generator GEN and normalised to $\sigma^{\mathrm{REF}}_{c\bar{c}}$ and $\sigma^{\mathrm{REF}}_{b\bar{b}}$ [93, 94]. The two fit parameters are the scaling factors $S_{c\bar{c}}$ and $S_{b\bar{b}}$, defined also as:

$$\sigma_{c\bar{c}} = S_{c\bar{c}} \cdot \sigma^{\mathrm{REF}}_{c\bar{c}}, \tag{5.2}$$

$$\sigma_{b\bar{b}} = S_{b\bar{b}} \cdot \sigma^{\mathrm{REF}}_{b\bar{b}}. \tag{5.3}$$

The e^+e^- spectra from heavy-flavour hadron decays are obtained by subtracting the expected cross section of e^+e^- pairs originating from vector meson and J/ψ decays, from the measured e^+e^- distributions. In the mass range 1.1–$2.7\,\mathrm{GeV}/c^2$ these contributions are
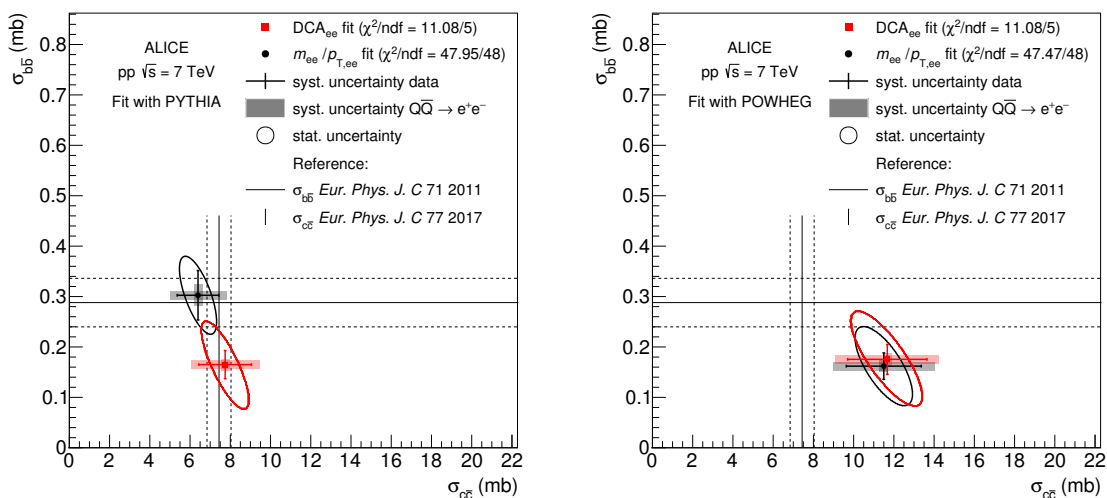
Figure 15. (Colour online) Total $c\bar{c}$ and $b\bar{b}$ cross sections extracted from a fit of the measured dielectron yield from heavy-flavour hadron decays in (m_{ee}, $p_{T,ee}$) and in DCA$_{ee}$ with PYTHIA (left) and POWHEG (right). The results and their uncertainties (see text) are compared to published cross sections, for which the total uncertainty is represented by dashed lines.

small, of the order of 4%. The fit is performed separately in DCA$_{ee}$ and in (m_{ee}, $p_{T,ee}$). For each combination of scaling factors, $S_{c\bar{c}}$ and $S_{b\bar{b}}$, the χ^2 value is calculated:

$$\chi^2 = \sum_{i=1}^{n} \left(\frac{x_i - \mu_i}{\sqrt{(\sigma_{x_i}^{\mathrm{stat}})^2 + (\sigma_{\mu_i}^{\mathrm{stat}})^2}} \right)^2 . \tag{5.4}$$

The values of the data points and MC calculations in bin i are given by x_i and μ_i, respectively, while $\sigma_{x_i}^{\mathrm{stat}}$ and $\sigma_{\mu_i}^{\mathrm{stat}}$ represent their statistical uncertainties. The result of the fit is determined by the minimum of χ^2. The extracted $\sigma_{c\bar{c}}$ and $\sigma_{b\bar{b}}$ cross sections are shown in figure 15 for the (m_{ee}, $p_{T,ee}$) and the DCA$_{ee}$ analysis when PYTHIA (left) or POWHEG (right) are used to calculate $f_{c\bar{c}}^{\mathrm{GEN}}$ and $f_{b\bar{b}}^{\mathrm{GEN}}$. The statistical uncertainties are plotted as ellipses and correspond to a confidence level of 68.3% (1σ) for each parameter (at $\chi^2 = \chi^2_{\min} + 1$ [101]). The error bars represent the systematic uncertainties determined by the fit result after moving the data points coherently up- and downward by their systematic uncertainties. The uncertainties of the effective beauty- and charm-to-electron branching ratios are shown as coloured bands. Finally the full and dashed lines show $\sigma_{c\bar{c}}^{\mathrm{REF}}$ [93] and $\sigma_{b\bar{b}}^{\mathrm{REF}}$ [94] with their total uncertainties. The statistical and systematic uncertainties are fully correlated between the PYTHIA- and POWHEG-based results, whereas they are partially correlated between the (m_{ee}, $p_{T,ee}$) and DCA$_{ee}$ fits. Both calculations, PYTHIA and POWHEG, are able to reproduce the (m_{ee}, $p_{T,ee}$) and DCA$_{ee}$ spectra reasonably well and give similar minimum χ^2 per number of degree of freedom (0.999 for POWHEG and 0.989 for PYTHIA for the (m_{ee}, $p_{T,ee}$) fit). The fit results of the (m_{ee}, $p_{T,ee}$) and DCA$_{ee}$ spectra are in agreement within the statistical and systematic uncertainties. The DCA$_{ee}$ distribution is slightly less sensitive to the total $b\bar{b}$ cross section. The e^+e^- pairs from beauty-

c$\bar{\text{c}}$	(m_{ee} , $p_{\text{T,ee}}$) fit	DCA$_{\text{ee}}$ fit
POWHEG	11.6 ±1.4 (stat.) ±1.9 (syst.) mb	11.7 ±1.8 (stat.) ±2.0 (syst.) mb
PYTHIA	6.4 ±0.9 (stat.) ±1.1 (syst.) mb	7.7 ±1.2 (stat.) ±1.3 (syst.) mb

Table 4. Summary of the total c$\bar{\text{c}}$ cross sections extracted from a fit of the measured dielectron spectra from heavy-flavour hadron decays in (m_{ee}, $p_{\text{T,ee}}$) and in DCA$_{\text{ee}}$ with PYTHIA and POWHEG. The uncertainty of 22% on the branching fractions and fragmentation functions (BR$_{\text{c}\to\text{e}}$) is not listed.

b$\bar{\text{b}}$	(m_{ee} , $p_{\text{T,ee}}$) fit	DCA$_{\text{ee}}$ fit
POWHEG	0.162 ±0.078 (stat.) ±0.026 (syst.) mb	0.175 ±0.092 (stat.) ±0.030 (syst.) mb
PYTHIA	0.303 ±0.077 (stat.) ±0.050 (syst.) mb	0.165 ±0.086 (stat.) ±0.028 (syst.) mb

Table 5. Summary of the total b$\bar{\text{b}}$ cross sections extracted from a fit of the measured dielectron spectra from heavy-flavour hadron decays in (m_{ee}, $p_{\text{T,ee}}$) and in DCA$_{\text{ee}}$ with PYTHIA and POWHEG. The uncertainty of 6% [89] on the branching fractions and fragmentation functions (BR$_{\text{b}(\to\text{c})\to\text{e}}$) is not listed.

hadron decays only dominate the last DCA$_{\text{ee}}$ bin (see figure 14). The shapes of the MC DCA$_{\text{ee}}$ templates are driven by the decay kinematics and assumed to be model independent. Therefore the extracted $\sigma_{\text{c}\bar{\text{c}}}$ and $\sigma_{\text{b}\bar{\text{b}}}$ directly reflect the different probabilities for the e$^+$e$^-$ pair to enter the detector acceptance calculated with PYTHIA or POWHEG (see table 3). The (m_{ee}, $p_{\text{T,ee}}$) fit depends in addition on the $p_{\text{T,ee}}$ distributions of correlated e$^+$e$^-$ pairs from charm and beauty-hadron decays, which are harder in POWHEG compared to PYTHIA. The total c$\bar{\text{c}}$ and b$\bar{\text{b}}$ cross sections show model dependences of about a factor of two. The fitted cross sections are summarised in tables 4 and 5. For comparison, the total c$\bar{\text{c}}$ cross section obtained by extrapolating in rapidity the D^0 p_{T} spectrum measured by the ALICE Collaboration [93] is of the order of 8.6 mb with POWHEG, and 7 mb with PYTHIA. The dielectron measurements can give further constraints on the MC event generators aiming to reproduce the heavy-flavour production mechanisms, once the uncertainties, which are fully correlated between the PYTHIA- and POWHEG-based results, are reduced.

5.1.4 J/ψ mass region

The mass region $2.7 < m_{\text{ee}} < 3.3\,\text{GeV}/c^2$ is dominated by J/ψ decays with a small contribution from charm-hadron decays. In the left panel of figure 16, the corresponding measured e$^+$e$^-$ cross section as a function of $p_{\text{T,ee}}$ is shown in comparison with the hadronic cocktail. Good agreement between data and cocktail is observed, as can be seen on the bottom left panel of figure 16 in the ratio of data to cocktail. The DCA$_{\text{ee}}$ distribution of e$^+$e$^-$ pairs is sensitive to the large decay length of B mesons ($c\tau_{\text{B}} \approx 470\,\mu\text{m}$) and the contribution from J/ψ originating from their decays. The measured DCA$_{\text{ee}}$ spectrum shown in the right panel of figure 16 cannot be reproduced with the MC template of the prompt J/ψ alone. The contribution from non-prompt J/ψ, together with those from correlated e$^+$e$^-$ pairs from heavy-flavour hadron decays, leads to a reasonable description of the data by the MC
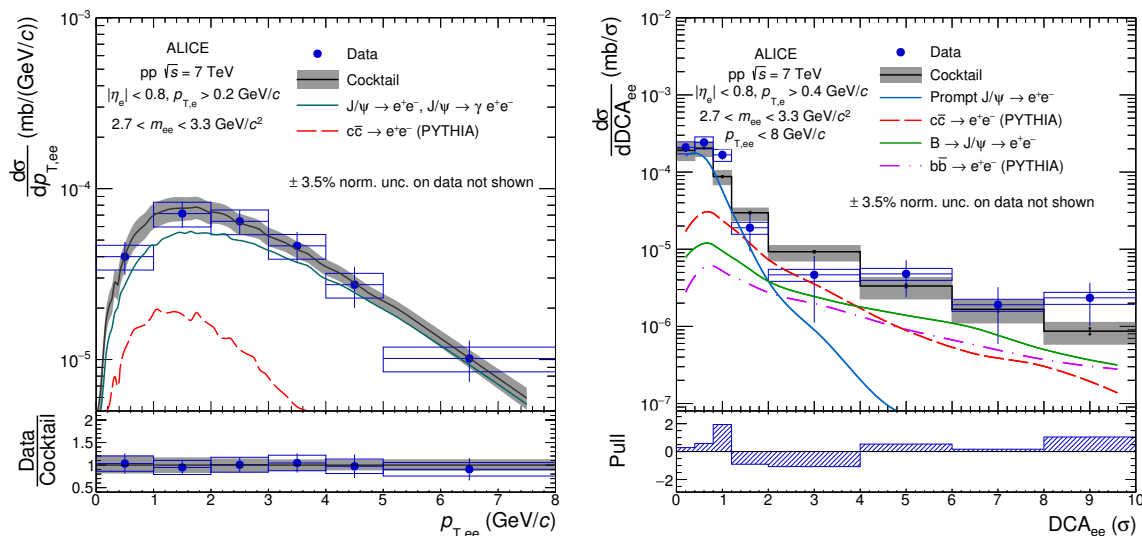
Figure 16. (Colour online) Inclusive e^+e^- cross section in pp collisions at $\sqrt{s} = 7\,\text{TeV}$ in the ALICE acceptance as a function of $p_{\text{T,ee}}$ (left panel) and DCA_{ee} (right panel) in the mass range $2.7 < m_{\text{ee}} < 3.3\,\text{GeV}/c^2$. The data are compared with a cocktail of expected sources. In the bottom panels, the ratio of data to cocktail as a function of $p_{\text{T,ee}}$ (left) and the pull distribution as a function of DCA_{ee} (right) are shown. Statistical and systematic uncertainties on the data are plotted as vertical bars and boxes, respectively. The total uncertainty of the cocktail is represented as a grey band.

calculations. The data are consistent with the fraction f_{B} of non-prompt J/ψ originating from B meson decays previously measured by the ALICE Collaboration [100].

5.2 Direct photons

Direct photons are defined as photons that do not originate from hadronic decays. In pp collisions, they are produced predominantly in hard partonic interactions and their production rate can be calculated with perturbative QCD.

The direct-photon cross section can be extracted from the measurement of real photons detected in the electromagnetic calorimeters or via photon conversion in the detector material of ALICE [29, 50]. For $p_{\text{T}} < 5\,\text{GeV}/c$, the extraction of the direct photon signal is difficult because of a large background from decay photons. An alternative way to measure direct-photon production is via its internal conversion into an e^+e^- pair. The advantage of this approach is that the main background originating from π^0 decays can be suppressed by selecting e^+e^- pairs with sufficiently large m_{ee} ($m_{\text{ee}} > m_{\pi^0}$). The drawback is the small internal conversion probability of $O(10^{-2})$ and the rapidly decreasing cross section as a function of m_{ee} ($\propto 1/m_{\text{ee}}$).

The mass dependence of the virtual-photon production for a given real-photon yield is given by the Kroll-Wada equation [70] which can be simplified in the case of $p_{\text{T,ee}}^2 \gg m_{\text{ee}}^2$, i.e. in the limit of quasi-real virtual photons, to:

$$\frac{\text{d}^2 N_{\text{ee}}}{\text{d}m_{\text{ee}}\text{d}p_{\text{T,ee}}} = \frac{2\alpha}{3\pi}\sqrt{1 - \frac{4m_{\text{e}}^2}{m_{\text{ee}}^2}}\left(1 + \frac{2m_{\text{e}}^2}{m_{\text{ee}}^2}\right)\cdot\frac{1}{m_{\text{ee}}}\frac{\text{d}N_\gamma}{\text{d}p_{\text{T}}}, \tag{5.5}$$
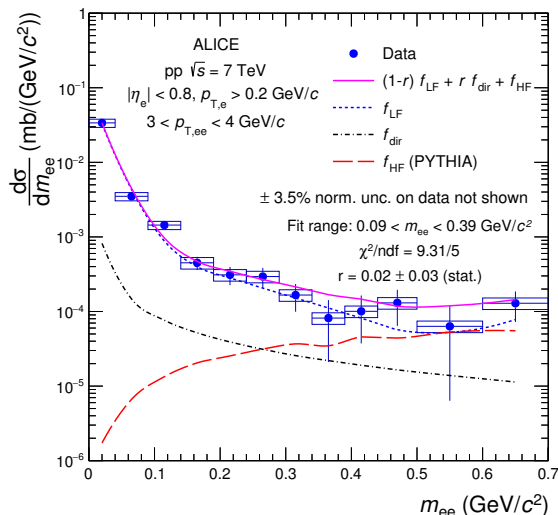
Figure 17. Fit of the e^+e^- cross section in pp collisions at $\sqrt{s} = 7\,\mathrm{TeV}$ in the ALICE acceptance as a function of m_{ee} in the range $3 < p_{T,ee} < 4\,\mathrm{GeV}/c$ with the three-component function defined by eq. (5.6). Statistical and systematic uncertainties on the data are shown separately as vertical bars and boxes, respectively.

with α, $\mathrm{d}N_\gamma/\mathrm{d}p_T$, and m_e being the fine-structure constant, the number of real photons at a given p_T ($= p_{T,ee}$), and the electron mass, respectively. To obtain the final expected shape $f_{\mathrm{dir}}(m_{ee})$ of the virtual direct photon mass distribution, the decay electrons are smeared by the detector resolution and passed through the acceptance of the ALICE barrel ($|\eta_e| < 0.8$, $p_{T,e} > 0.2\,\mathrm{GeV}/c$).

The measured m_{ee} distributions of e^+e^- pairs are fitted in different $p_{T,ee}$ bins with a three-component function:

$$f(m_{ee}, r) = (1-r)f_{\mathrm{LF}}(m_{ee}) + r\,f_{\mathrm{dir}}(m_{ee}) + f_{\mathrm{HF}}(m_{ee}), \qquad (5.6)$$

where f_{LF} is the shape of the mass distribution of the light-flavour component of the hadronic cocktail and f_{HF} is the e^+e^- cross section of the expected heavy-flavour contribution in the corresponding $p_{T,ee}$ bin. The ratio r of direct to inclusive photons is the only fit parameter. The fit is limited to the mass range $0.09 < m_{ee} < 0.39\,\mathrm{GeV}/c^2$ to ensure the condition $p_{T,ee}^2 \gg m_{ee}^2$. Both f_{LF} and f_{dir} are normalised such that they separately fit the data for $m_{ee} < 0.04\,\mathrm{GeV}/c^2$, because in this mass region the functional shapes of f_{LF} and f_{dir} are essentially identical. In figure 17, the measured m_{ee}-differential e^+e^- cross section is shown in the $p_{T,ee}$ range $3 < p_{T,ee} < 4\,\mathrm{GeV}/c$, together with the fit result. The individual components are plotted separately. The systematic uncertainties due to the model dependence of the estimated e^+e^- yield from $c\bar{c}$ is evaluated by repeating the fit with f_{HF} computed with the POWHEG generator and found to be below 0.75% in the full p_T range.

The following sources of systematic uncertainty are considered: (1) the fit range, (2) the systematic uncertainties of the data, (3) the ones of the hadronic cocktail components, and (4) the normalisation range. The fit is thus repeated in different mass intervals between

p_T interval	Upper limits at 90% C.L. on $R_\gamma = \sigma_{\text{inclusive}}^\gamma / \sigma_{\text{decay}}^\gamma$
$1 < p_T < 1.5\,\text{GeV}/c$	1.035
$1.5 < p_T < 2\,\text{GeV}/c$	1.027
$2 < p_T < 3\,\text{GeV}/c$	1.030
$3 < p_T < 4\,\text{GeV}/c$	1.096
$4 < p_T < 8\,\text{GeV}/c$	1.197

Table 6. Upper limits at 90% C.L. on the ratio of inclusive to decay photon cross sections.

$0.09\,\text{GeV}/c^2$ and $0.39\,\text{GeV}/c^2$. The corresponding uncertainty is found to be relevant only in the p_T intervals 2–3 GeV/c and 3–4 GeV/c. The uncertainty arising from the systematic uncertainties of the data is evaluated by shifting all data points coherently to the upper and lower limits of their systematic uncertainties and by repeating the fit procedure. The systematic uncertainties from the light-flavour and heavy-flavour cocktail components are similarly estimated. The contribution of each light-flavour dielectron source is moved separately to its upper and lower systematic uncertainties. The largest source of uncertainty originates from the η/π^0 ratio. In most of the $p_{T,ee}$ bins, this is the dominant source of systematic uncertainties. Finally, f_{LF} and f_{dir} are normalised to the data in the range $0 < m_{ee} < 0.09\,\text{GeV}/c^2$ to evaluate the normalisation uncertainty. All systematic uncertainties are added in quadrature to obtain the total systematic uncertainty. In figure 18, the ratio of inclusive to decay photon cross sections, i.e. $R_\gamma = \sigma_{\text{inclusive}}^\gamma / \sigma_{\text{decay}}^\gamma = 1/(1-r)$, is shown as a function of p_T. It is consistent with unity within the statistical and systematic uncertainties. Perturbative QCD calculations at NLO [102] performed with the CT10 PDFs [103–105] predict a small ratio of inclusive to decay photon cross sections over the measured p_T range, compatible with the measurements within uncertainties. The uncertainty band of the calculation is given by the simultaneous variation of the factorisation, renormalisation, and fragmentation scales (with $0.5 p_T < \mu_F < 2 p_T$ for the factorization scale) used in the calculation. The upper limits at 90% confidence level (C.L.) on R_γ, extracted with the Feldman-Cousins method [106], are summarised in table. 6. Gaussian distributions are assumed for statistical and systematic uncertainties, which are treated independently and summed in quadrature. The results are consistent with the R_γ measured in pp collisions at $\sqrt{s} = 8\,\text{TeV}$ with the real photon analysis performed by the ALICE Collaboration [29].

6 Conclusion

A measurement of e^+e^- pair production at mid-rapidity ($|\eta_e| < 0.8$) in minimum bias pp collisions at $\sqrt{s} = 7\,\text{TeV}$ with ALICE at the LHC is shown. The results are presented as a function of the invariant mass m_{ee} ($0 < m_{ee} < 3.3\,\text{GeV}/c^2$) of the e^+e^- pair, its transverse momentum $p_{T,ee}$ ($0 < p_{T,ee} < 8\,\text{GeV}/c$), and the pair transverse impact parameter DCA_{ee}.
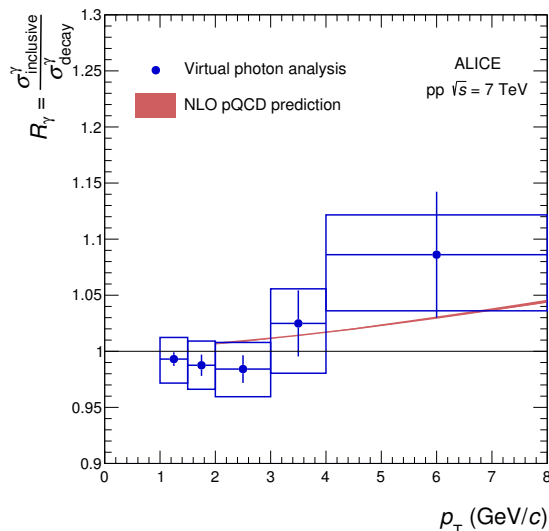
Figure 18. Ratio of inclusive to decay photon cross sections extracted from the dielectron spectra measured in pp collisions at $\sqrt{s} = 7\,\mathrm{TeV}$. The results are compared with NLO pQCD calculations [102–105]. Statistical and systematic uncertainties are shown as vertical bars and boxes for the data, respectively, and as a band for the NLO pQCD calculations.

The data are compared with a hadronic cocktail composed of the expected dielectron cross sections from the known hadronic sources. The contributions from semileptonic decays of heavy-flavour hadrons are calculated with PYTHIA and POWHEG, and normalised to the measured total $c\bar{c}$ and $b\bar{b}$ cross sections [93, 94]. The shape of the DCA_{ee} distribution of each source is obtained using a full simulation of the ALICE detector. The obtained DCA_{ee} templates are normalised to the cocktail calculations integrated over the same m_{ee} and $p_{T,ee}$ range.

Overall good agreement between data and cocktail is observed for all m_{ee}, $p_{T,ee}$, and DCA_{ee} intervals considered. In the π^0 mass region ($m_{ee} < 0.14\,\mathrm{GeV}/c^2$), the comparison of the measured DCA_{ee} distribution with the MC templates shows that the detector resolution is well reproduced in the simulations. In the low-mass region ($0.14 < m_{ee} < 1.1\,\mathrm{GeV}/c^2$), prompt and non-prompt contributions can be separated with the DCA_{ee} observable. In the intermediate-mass region, $1.1 < m_{ee} < 2.7\,\mathrm{GeV}/c^2$, the measured e^+e^- cross section is dominated by correlated e^+e^- pairs from charm- and beauty-hadron decays. The $c\bar{c}$ and $b\bar{b}$ total cross sections can be extracted from the data by a double-differential fit of the measured spectra in (m_{ee}, $p_{T,ee}$) and by fitting the DCA_{ee} distribution in the IMR. Both fits give consistent results within statistical and systematic uncertainties. The extracted cross sections show a large model-dependence between PYTHIA and POWHEG by up to a factor of two. In the J/ψ mass region ($2.7 < m_{ee} < 3.3\,\mathrm{GeV}/c^2$), the measured DCA_{ee}- and $p_{T,ee}$-differential cross sections are well described by the hadronic cocktail. The DCA_{ee} distribution is sensitive to the fraction f_B of non-prompt J/ψ originating from B-meson decays. The data are consistent with the previously measured f_B by the ALICE Collaboration [100].

In the quasi-real virtual-photon region, at low mass ($m_{ee} < 0.4\,\mathrm{GeV}/c^2$) and high $p_{T,ee}$ ($p_{T,ee} > 1\,\mathrm{GeV}/c$), the contribution of virtual direct photons is extracted from the data

by fitting the m_{ee} distributions in $p_{T,ee}$ bins. The extracted ratio of the inclusive-to-decay photon cross sections is found to be consistent with predictions from pQCD calculations at NLO [102–105] within statistical and systematic uncertainties.

The e^+e^- pair production will be further studied in pp, p−Pb and Pb-Pb collisions with the LHC Run 2 data, which are currently recorded, as well as with the expected high-statistics data from the LHC Run 3 starting in 2021 [107–110]. In particular, the measurement of the DCA_{ee} spectra in Run 3 will benefit from the new Inner Tracking System [110] with a smaller material budget and a resulting higher impact parameter resolution, while the upgrade of the Time Projection Chamber will provide a significant increase of the statistics [108, 109].

Acknowledgments

References

[1] ALICE collaboration, *ALICE: physics performance report, volume I*, *J. Phys.* **G 30** (2004) 1517 [[INSPIRE](https://inspirehep.net/)].

[2] ALICE collaboration, *ALICE: physics performance report, volume II*, *J. Phys.* **G 32** (2006) 1295 [[INSPIRE](https://inspirehep.net/)].

[3] ALICE collaboration, *The ALICE experiment at the CERN LHC*, 2008 *JINST* **3** S08002 [[INSPIRE](https://inspirehep.net/)].

[4] F. Karsch, *Lattice simulations of the thermodynamics of strongly interacting elementary particles and the exploration of new phases of matter in relativistic heavy ion collisions*, *J. Phys. Conf. Ser.* **46** (2006) 122 [[hep-lat/0608003](https://arxiv.org/abs/hep-lat/0608003)] [[INSPIRE](https://inspirehep.net/)].

[5] WUPPERTAL-BUDAPEST collaboration, S. Borsányi et al., *Is there still any T_c mystery in lattice QCD? Results with physical masses in the continuum limit III*, *JHEP* **09** (2010) 073 [arXiv:1005.3508] [INSPIRE].

[6] S. Borsányi et al., *The QCD equation of state with dynamical quarks*, *JHEP* **11** (2010) 077 [arXiv:1007.2580] [INSPIRE].

[7] A. Bazavov et al., *The chiral and deconfinement aspects of the QCD transition*, *Phys. Rev.* **D 85** (2012) 054503 [arXiv:1111.1710] [INSPIRE].

[8] P. Petreczky, *Review of recent highlights in lattice calculations at finite temperature and finite density*, PoS(Confinement X)028 [arXiv:1301.6188] [INSPIRE].

[9] R. Rapp, J. Wambach and H. van Hees, *The chiral restoration transition of QCD and low mass dileptons*, *Landolt-Bornstein* **23** (2010) 134 [arXiv:0901.3289] [INSPIRE].

[10] I. Tserruya, *Electromagnetic probes*, *Landolt-Bornstein* **23** (2010) 176 [arXiv:0903.0415] [INSPIRE].

[11] F.-M. Liu and S.-X. Liu, *Quark-gluon plasma formation time and direct photons from heavy ion collisions*, *Phys. Rev.* **C 89** (2014) 034906 [arXiv:1212.6587] [INSPIRE].

[12] P. Petreczky, *Lattice QCD at non-zero temperature*, *J. Phys.* **G 39** (2012) 093002 [arXiv:1203.5320] [INSPIRE].

[13] C.A. Dominguez, M. Loewe and Y. Zhang, *Chiral symmetry restoration and deconfinement in QCD at finite temperature*, *Phys. Rev.* **D 86** (2012) 034030 [*Erratum ibid.* **D 90** (2014) 039903] [arXiv:1205.3361] [INSPIRE].

[14] P.M. Hohler and R. Rapp, *Is ρ-meson melting compatible with chiral restoration?*, *Phys. Lett.* **B 731** (2014) 103 [arXiv:1311.2921] [INSPIRE].

[15] M. Gyulassy and M. Plumer, *Jet quenching in dense matter*, *Phys. Lett.* **B 243** (1990) 432 [INSPIRE].

[16] R. Baier, Y.L. Dokshitzer, A.H. Mueller, S. Peigné and D. Schiff, *Radiative energy loss and p_T broadening of high-energy partons in nuclei*, *Nucl. Phys.* **B 484** (1997) 265 [hep-ph/9608322] [INSPIRE].

[17] M.H. Thoma and M. Gyulassy, *Quark damping and energy loss in the high temperature QCD*, *Nucl. Phys.* **B 351** (1991) 491 [INSPIRE].

[18] E. Braaten and M.H. Thoma, *Energy loss of a heavy fermion in a hot plasma*, *Phys. Rev.* **D 44** (1991) 1298 [INSPIRE].

[19] E. Braaten and M.H. Thoma, *Energy loss of a heavy quark in the quark-gluon plasma*, *Phys. Rev.* **D 44** (1991) R2625 [INSPIRE].

[20] V. Greco, C.M. Ko and R. Rapp, *Quark coalescence for charmed mesons in ultrarelativistic heavy ion collisions*, *Phys. Lett.* **B 595** (2004) 202 [nucl-th/0312100] [INSPIRE].

[21] A. Andronic, P. Braun-Munzinger, K. Redlich and J. Stachel, *Statistical hadronization of charm in heavy ion collisions at SPS, RHIC and LHC*, *Phys. Lett.* **B 571** (2003) 36 [nucl-th/0303036] [INSPIRE].

[22] S. Batsouli, S. Kelly, M. Gyulassy and J.L. Nagle, *Does the charm flow at RHIC?*, *Phys. Lett.* **B 557** (2003) 26 [nucl-th/0212068] [INSPIRE].

[23] PHENIX collaboration, A. Adare et al., *Dilepton mass spectra in $p + p$ collisions at $\sqrt{s} = 200$ GeV and the contribution from open charm*, *Phys. Lett.* **B 670** (2009) 313 [arXiv:0802.0050] [INSPIRE].

[24] PHENIX collaboration, A. Adare et al., *Detailed measurement of the e^+e^- pair continuum in $p + p$ and $Au + Au$ collisions at $\sqrt{s_{NN}} = 200$ GeV and implications for direct photon production*, *Phys. Rev.* **C 81** (2010) 034911 [arXiv:0912.0244] [INSPIRE].

[25] STAR collaboration, L. Adamczyk et al., *Di-electron spectrum at mid-rapidity in $p + p$ collisions at $\sqrt{s} = 200$ GeV*, *Phys. Rev.* **C 86** (2012) 024906 [arXiv:1204.1890] [INSPIRE].

[26] PHENIX collaboration, A. Adare et al., *Cross section for $b\bar{b}$ production via dielectrons in $d + Au$ collisions at $\sqrt{s_{NN}} = 200$ GeV*, *Phys. Rev.* **C 91** (2015) 014907 [arXiv:1405.4004] [INSPIRE].

[27] PHENIX collaboration, A. Adare et al., *Measurements of e^+e^- pairs from open heavy flavor in $p + p$ and $d + A$ collisions at $\sqrt{s_{NN}} = 200$ GeV*, *Phys. Rev.* **C 96** (2017) 024907 [arXiv:1702.01084] [INSPIRE].

[28] PHENIX collaboration, A. Adare et al., *Direct photon production in $d + Au$ collisions at $\sqrt{s_{NN}} = 200$ GeV*, *Phys. Rev.* **C 87** (2013) 054907 [arXiv:1208.1234] [INSPIRE].

[29] ALICE collaboration, *Direct photon production at low transverse momentum in proton-proton collisions at $\sqrt{s} = 2.76$ and 8 TeV*, arXiv:1803.09857 [INSPIRE].

[30] CERES collaboration, G. Agakichiev et al., *Enhanced production of low mass electron pairs in 200 GeV/u S-Au collisions at the CERN SPS*, *Phys. Rev. Lett.* **75** (1995) 1272 [INSPIRE].

[31] CERES/NA45 collaboration, G. Agakishiev et al., *Low mass e^+e^- pair production in 158 A-GeV Pb-Au collisions at the CERN SPS, its dependence on multiplicity and transverse momentum*, *Phys. Lett.* **B 422** (1998) 405 [nucl-ex/9712008] [INSPIRE].

[32] D. Adamova et al., *Modification of the rho-meson detected by low-mass electron-positron pairs in central Pb-Au collisions at 158 A-GeV/c*, *Phys. Lett.* **B 666** (2008) 425 [nucl-ex/0611022] [INSPIRE].

[33] CERES/NA45 collaboration, D. Adamova et al., *Enhanced production of low mass electron pairs in 40 AGeV Pb-Au collisions at the CERN SPS*, *Phys. Rev. Lett.* **91** (2003) 042301 [nucl-ex/0209024] [INSPIRE].

[34] NA60 collaboration, R. Arnaldi et al., *First measurement of the rho spectral function in high-energy nuclear collisions*, *Phys. Rev. Lett.* **96** (2006) 162302 [nucl-ex/0605007] [INSPIRE].

[35] NA60 collaboration, R. Arnaldi et al., *NA60 results on thermal dimuons*, *Eur. Phys. J.* **C 61** (2009) 711 [arXiv:0812.3053] [INSPIRE].

[36] PHENIX collaboration, A. Adare et al., *Dielectron production in $Au + Au$ collisions at $\sqrt{s_{NN}} = 200$ GeV*, *Phys. Rev.* **C 93** (2016) 014904 [arXiv:1509.04667] [INSPIRE].

[37] STAR collaboration, L. Adamczyk et al., *Dielectron mass spectra from $Au + Au$ collisions at $\sqrt{s_{NN}} = 200$ GeV*, *Phys. Rev. Lett.* **113** (2014) 022301 [*Addendum ibid.* **113** (2014) 049903] [arXiv:1312.7397] [INSPIRE].

[38] STAR collaboration, L. Adamczyk et al., *Measurements of dielectron production in $Au + Au$ collisions at $\sqrt{s_{NN}} = 200$ GeV from the STAR experiment*, *Phys. Rev.* **C 92** (2015) 024912 [arXiv:1504.01317] [INSPIRE].

[39] H. van Hees and R. Rapp, *Dilepton radiation at the CERN Super Proton Synchrotron*, *Nucl. Phys.* **A 806** (2008) 339 [arXiv:0711.3444] [ɪɴSPIRE].

[40] H. van Hees and R. Rapp, *Comprehensive interpretation of thermal dileptons at the SPS*, *Phys. Rev. Lett.* **97** (2006) 102301 [hep-ph/0603084] [ɪɴSPIRE].

[41] J. Ruppert, C. Gale, T. Renk, P. Lichard and J.I. Kapusta, *Low mass dimuons produced in relativistic nuclear collisions*, *Phys. Rev. Lett.* **100** (2008) 162301 [arXiv:0706.1934] [ɪɴSPIRE].

[42] K. Dusling, D. Teaney and I. Zahed, *Thermal dimuon yields at NA60*, *Phys. Rev.* **C 75** (2007) 024908 [nucl-th/0604071] [ɪɴSPIRE].

[43] E.L. Bratkovskaya, W. Cassing and O. Linnyk, *Low mass dilepton production at ultrarelativistic energies*, *Phys. Lett.* **B 670** (2009) 428 [arXiv:0805.3177] [ɪɴSPIRE].

[44] O. Linnyk, E.L. Bratkovskaya, V. Ozvenchuk, W. Cassing and C.M. Ko, *Dilepton production in nucleus-nucleus collisions at top SPS energy within the Parton-Hadron-String Dynamics (PHSD) transport approach*, *Phys. Rev.* **C 84** (2011) 054917 [arXiv:1107.3402] [ɪɴSPIRE].

[45] R. Rapp and J. Wambach, *Low mass dileptons at the CERN SPS: evidence for chiral restoration?*, *Eur. Phys. J.* **A 6** (1999) 415 [hep-ph/9907502] [ɪɴSPIRE].

[46] R. Rapp, *Signatures of thermal dilepton radiation at RHIC*, *Phys. Rev.* **C 63** (2001) 054907 [hep-ph/0010101] [ɪɴSPIRE].

[47] R. Rapp, *Dilepton spectroscopy of QCD matter at collider energies*, *Adv. High Energy Phys.* **2013** (2013) 148253 [arXiv:1304.2309] [ɪɴSPIRE].

[48] K. Dusling and I. Zahed, *Low mass dilepton radiation at RHIC*, *Nucl. Phys.* **A 825** (2009) 212 [arXiv:0712.1982] [ɪɴSPIRE].

[49] W. Liu and R. Rapp, *Low-energy thermal photons from meson-meson bremsstrahlung*, *Nucl. Phys.* **A 796** (2007) 101 [nucl-th/0604031] [ɪɴSPIRE].

[50] ALICE collaboration, *Direct photon production in Pb-Pb collisions at $\sqrt{s_{\rm NN}} = 2.76\,TeV$*, *Phys. Lett.* **B 754** (2016) 235 [arXiv:1509.07324] [ɪɴSPIRE].

[51] R. Shahoyan, *Evidence for the production of thermal dimuons with masses above $1\,GeV/c^2$ in 158 A-GeV In-In collisions*, *Nucl. Phys.* **A 827** (2009) 353C [ɪɴSPIRE].

[52] NA60 collaboration, R. Arnaldi et al., *Evidence for radial flow of thermal dileptons in high-energy nuclear collisions*, *Phys. Rev. Lett.* **100** (2008) 022302 [arXiv:0711.1816] [ɪɴSPIRE].

[53] T. Renk and J. Ruppert, *Dimuon transverse momentum spectra as a tool to characterize the emission region in heavy-ion collisions*, *Phys. Rev.* **C 77** (2008) 024907 [hep-ph/0612113] [ɪɴSPIRE].

[54] T. Sjöstrand, S. Mrenna and P.Z. Skands, *PYTHIA 6.4 physics and manual*, *JHEP* **05** (2006) 026 [hep-ph/0603175] [ɪɴSPIRE].

[55] P. Nason, *A new method for combining NLO QCD with shower Monte Carlo algorithms*, *JHEP* **11** (2004) 040 [hep-ph/0409146] [ɪɴSPIRE].

[56] S. Frixione, P. Nason and C. Oleari, *Matching NLO QCD computations with parton shower simulations: the POWHEG method*, *JHEP* **11** (2007) 070 [arXiv:0709.2092] [ɪɴSPIRE].

[57] S. Alioli, P. Nason, C. Oleari and E. Re, *A general framework for implementing NLO calculations in shower Monte Carlo programs: the POWHEG BOX*, *JHEP* **06** (2010) 043 [arXiv:1002.2581] [INSPIRE].

[58] S. Frixione, P. Nason and G. Ridolfi, *A positive-weight next-to-leading-order Monte Carlo for heavy flavour hadroproduction*, *JHEP* **09** (2007) 126 [arXiv:0707.3088] [INSPIRE].

[59] ALICE collaboration, *Performance of the ALICE experiment at the CERN LHC*, *Int. J. Mod. Phys.* **A 29** (2014) 1430044 [arXiv:1402.4476] [INSPIRE].

[60] ALICE collaboration, *Alignment of the ALICE inner tracking system with cosmic-ray tracks*, 2010 *JINST* **5** P03003 [arXiv:1001.0502] [INSPIRE].

[61] J. Alme et al., *The ALICE TPC, a large 3-dimensional tracking device with fast readout for ultra-high multiplicity events*, *Nucl. Instrum. Meth.* **A 622** (2010) 316 [arXiv:1001.1950] [INSPIRE].

[62] A. Akindinov et al., *Performance of the ALICE time-of-flight detector at the LHC*, *Eur. Phys. J. Plus* **128** (2013) 44 [INSPIRE].

[63] ALICE collaboration, *Performance of the ALICE VZERO system*, 2013 *JINST* **8** P10016 [arXiv:1306.3130] [INSPIRE].

[64] ALICE collaboration, *Measurement of inelastic, single- and double-diffraction cross sections in proton-proton collisions at the LHC with ALICE*, *Eur. Phys. J.* **C 73** (2013) 2456 [arXiv:1208.4968] [INSPIRE].

[65] ALICE collaboration, *Measurement of electrons from semileptonic heavy-flavour hadron decays in pp collisions at $\sqrt{s} = 7\,TeV$*, *Phys. Rev.* **D 86** (2012) 112007 [arXiv:1205.5423] [INSPIRE].

[66] R. Fruhwirth, *Application of Kalman filtering to track and vertex fitting*, *Nucl. Instrum. Meth.* **A 262** (1987) 444 [INSPIRE].

[67] P.Z. Skands, *Tuning Monte Carlo generators: the Perugia tunes*, *Phys. Rev.* **D 82** (2010) 074018 [arXiv:1005.3457] [INSPIRE].

[68] R. Brun, R. Hagelberg, M. Hansroul and J.C. Lassalle, *GEANT: simulation program for particle physics experiments. User guide and reference manual*, CERN-DD-78-2, CERN, Geneva, Switzerland, (1978) [INSPIRE].

[69] ALICE collaboration, *Momentum transformation matrix for dielectron simulations in Pb-Pb collisions at $\sqrt{s_{NN}} = 2.76\,TeV$*, ALICE-PUBLIC-2017-011, CERN, Geneva, Switzerland, (2017).

[70] N.M. Kroll and W. Wada, *Internal pair production associated with the emission of high-energy gamma rays*, *Phys. Rev.* **98** (1955) 1355 [INSPIRE].

[71] L.G. Landsberg, *Electromagnetic decays of light mesons*, *Phys. Rept.* **128** (1985) 301 [INSPIRE].

[72] R.I. Dzhelyadin et al., *Study of the electromagnetic transition form-factor in $\omega \to \pi^0 \mu^+ \mu^-$ decay*, *Phys. Lett.* **B 102** (1981) 296 [*JETP Lett.* **33** (1981) 228] [INSPIRE].

[73] NA60 collaboration, R. Arnaldi et al., *Precision study of the $\eta \to \mu^+\mu^-\gamma$ and $\omega \to \mu^+\mu^-\pi^0$ electromagnetic transition form-factors and of the $\rho \to \mu^+\mu^-$ line shape in NA60*, *Phys. Lett.* **B 757** (2016) 437 [arXiv:1608.07898] [INSPIRE].

[74] NA60 collaboration, R. Arnaldi et al., *Study of the electromagnetic transition form-factors in $\eta \to \mu^+\mu^-\gamma$ and $\omega \to \mu^+\mu^-\pi^0$ decays with NA60*, *Phys. Lett.* **B 677** (2009) 260 [arXiv:0902.2547] [INSPIRE].

[75] J. Knoll, *Transport dynamics of broad resonances*, *Prog. Part. Nucl. Phys.* **42** (1999) 177 [nucl-th/9811099] [INSPIRE].

[76] G.J. Gounaris and J.J. Sakurai, *Finite width corrections to the vector meson dominance prediction for $\rho \to e^+e^-$*, *Phys. Rev. Lett.* **21** (1968) 244 [INSPIRE].

[77] ALICE collaboration, *Multiplicity dependence of charged pion, kaon and (anti)proton production at large transverse momentum in p-Pb collisions at $\sqrt{s_{\mathrm{NN}}} = 5.02$ TeV*, *Phys. Lett.* **B 760** (2016) 720 [arXiv:1601.03658] [INSPIRE].

[78] ALICE collaboration, *Neutral pion and η meson production in proton-proton collisions at $\sqrt{s} = 0.9$ TeV and $\sqrt{s} = 7$ TeV*, *Phys. Lett.* **B 717** (2012) 162 [arXiv:1205.5724] [INSPIRE].

[79] ALICE collaboration, *Production of $K^*(892)^0$ and $\phi(1020)$ in pp collisions at $\sqrt{s} = 7$ TeV*, *Eur. Phys. J.* **C 72** (2012) 2183 [arXiv:1208.5717] [INSPIRE].

[80] ALICE collaboration, *Rapidity and transverse momentum dependence of inclusive J/ψ production in pp collisions at $\sqrt{s} = 7$ TeV*, *Phys. Lett.* **B 704** (2011) 442 [*Erratum ibid.* **B 718** (2012) 692] [arXiv:1105.0380] [INSPIRE].

[81] M. Biyajima, T. Mizoguchi, N. Nakajima, N. Suzuki and G. Wilk, *Modified Hagedorn formula including temperature fluctuation — estimation of temperatures at RHIC experiments*, *Eur. Phys. J.* **C 48** (2006) 597 [hep-ph/0602120] [INSPIRE].

[82] WA80 collaboration, R. Albrecht et al., *Production of eta mesons in $200\,A/GeV$ S+S and S+Au reactions*, *Phys. Lett.* **B 361** (1995) 14 [hep-ex/9507009] [INSPIRE].

[83] P.K. Khandai, P. Shukla and V. Singh, *Meson spectra and m_T scaling in $p + p$, $d+Au$ and $Au+Au$ collisions at $\sqrt{s_{\mathrm{NN}}} = 200$ GeV*, *Phys. Rev.* **C 84** (2011) 054904 [arXiv:1110.3929] [INSPIRE].

[84] L. Altenkämper, F. Bock, C. Loizides and N. Schmidt, *Applicability of transverse mass scaling in hadronic collisions at energies available at the CERN Large Hadron Collider*, *Phys. Rev.* **C 96** (2017) 064907 [arXiv:1710.01933] [INSPIRE].

[85] ALICE collaboration, *Production of $\omega(782)$ in pp collisions at $\sqrt{s} = 7$ TeV*, ALICE-PUBLIC-2018-004, CERN, Geneva, Switzerland, (2018).

[86] ALICE collaboration, *Production of the $\rho(770)^0$ meson in pp and Pb-Pb collisions at $\sqrt{s_{\mathrm{NN}}} = 2.76$ TeV*, CERN-EP-2018-106, CERN, Geneva, Switzerland, (2018) [arXiv:1805.04365] [INSPIRE].

[87] T. Sjöstrand, S. Mrenna and P.Z. Skands, *A brief introduction to PYTHIA 8.1*, *Comput. Phys. Commun.* **178** (2008) 852 [arXiv:0710.3820] [INSPIRE].

[88] P. Skands, S. Carrazza and J. Rojo, *Tuning PYTHIA 8.1: the Monash 2013 tune*, *Eur. Phys. J.* **C 74** (2014) 3024 [arXiv:1404.5630] [INSPIRE].

[89] M. Tanabashi et al., *Review of particle physics*, *Phys. Rev.* **D 98** (2018) 030001 [INSPIRE].

[90] CTEQ collaboration, H.L. Lai et al., *Global QCD analysis of parton structure of the nucleon: CTEQ5 parton distributions*, *Eur. Phys. J.* **C 12** (2000) 375 [hep-ph/9903282] [INSPIRE].

[91] G. Corcella et al., *HERWIG 6: an event generator for hadron emission reactions with interfering gluons (including supersymmetric processes)*, *JHEP* **01** (2001) 010 [hep-ph/0011363] [INSPIRE].

[92] P.M. Nadolsky et al., *Implications of CTEQ global analysis for collider observables*, *Phys. Rev.* **D 78** (2008) 013004 [arXiv:0802.0007] [INSPIRE].

[93] ALICE collaboration, *Measurement of D-meson production at mid-rapidity in pp collisions at $\sqrt{s} = 7$ TeV*, *Eur. Phys. J.* **C 77** (2017) 550 [arXiv:1702.00766] [INSPIRE].

[94] LHCb collaboration, *Measurement of J/ψ production in pp collisions at $\sqrt{s} = 7$ TeV*, *Eur. Phys. J.* **C 71** (2011) 1645 [arXiv:1103.0423] [INSPIRE].

[95] ALICE collaboration, *Λ_c^+ production in pp collisions at $\sqrt{s} = 7$ TeV and in p-Pb collisions at $\sqrt{s_{NN}} = 5.02$ TeV*, *JHEP* **04** (2018) 108 [arXiv:1712.09581] [INSPIRE].

[96] L. Gladilin, *Fragmentation fractions of c and b quarks into charmed hadrons at LEP*, *Eur. Phys. J.* **C 75** (2015) 19 [arXiv:1404.3888] [INSPIRE].

[97] M. Cacciari, M. Greco and P. Nason, *The p_T spectrum in heavy flavor hadroproduction*, *JHEP* **05** (1998) 007 [hep-ph/9803400] [INSPIRE].

[98] ALICE collaboration, *Measurement of electrons from beauty hadron decays in pp collisions at $\sqrt{s} = 7$ TeV*, *Phys. Lett.* **B 721** (2013) 13 [*Erratum ibid.* **B 763** (2016) 507] [arXiv:1208.1902] [INSPIRE].

[99] ALICE collaboration, *D_s^+ meson production at central rapidity in proton-proton collisions at $\sqrt{s} = 7$ TeV*, *Phys. Lett.* **B 718** (2012) 279 [arXiv:1208.1948] [INSPIRE].

[100] ALICE collaboration, *Measurement of prompt J/ψ and beauty hadron production cross sections at mid-rapidity in pp collisions at $\sqrt{s} = 7$ TeV*, *JHEP* **11** (2012) 065 [arXiv:1205.5880] [INSPIRE].

[101] W. Press, S. Teukolsky, W. Vetterling and B. Flannery, *Numerical recipes in C: the art of scientific computing*, Press Syndicate of the University of Cambridge, https://www2.units.it/ipl/students_area/imm2/files/Numerical_Recipes.pdf, Cambridge, U.K., (1992).

[102] L.E. Gordon and W. Vogelsang, *Polarized and unpolarized prompt photon production beyond the leading order*, *Phys. Rev.* **D 48** (1993) 3136 [INSPIRE].

[103] H.-L. Lai et al., *New parton distributions for collider physics*, *Phys. Rev.* **D 82** (2010) 074024 [arXiv:1007.2241] [INSPIRE].

[104] J. Gao et al., *CT10 next-to-next-to-leading order global analysis of QCD*, *Phys. Rev.* **D 89** (2014) 033009 [arXiv:1302.6246] [INSPIRE].

[105] M. Guzzi, P. Nadolsky, E. Berger, H.-L. Lai, F. Olness and C.P. Yuan, *CT10 parton distributions and other developments in the global QCD analysis*, arXiv:1101.0561 [INSPIRE].

[106] G.J. Feldman and R.D. Cousins, *A unified approach to the classical statistical analysis of small signals*, *Phys. Rev.* **D 57** (1998) 3873 [physics/9711021] [INSPIRE].

[107] ALICE collaboration, *Technical design report for the upgrade of the online-offline computing system*, CERN-LHCC-2015-006, CERN, Geneva, Switzerland, (2015) [ALICE-TDR-019].

[108] ALICE collaboration, *Upgrade of the ALICE time projection chamber*, CERN-LHCC-2013-020, CERN, Geneva, Switzerland, (2013) [ALICE-TDR-016].

[109] ALICE collaboration, *Addendum to the technical design report for the upgrade of the ALICE time projection chamber*, CERN-LHCC-2015-002, CERN, Geneva, Switzerland, (2015) [ALICE-TDR-016-ADD-1].

[110] ALICE collaboration, *Upgrade of the inner tracking system conceptual design report*, CERN-LHCC-2012-013, CERN, Geneva, Switzerland, (2012) [LHCC-P-005].

The ALICE collaboration

S. Acharya[139] , F.T.-. Acosta[22] , D. Adamová[94] , J. Adolfsson[81] , M.M. Aggarwal[98] , G. Aglieri Rinella[36] , M. Agnello[33] , N. Agrawal[49] , Z. Ahammed[139] , S.U. Ahn[77] , S. Aiola[144] , A. Akindinov[65] , M. Al-Turany[104] , S.N. Alam[139] , D.S.D. Albuquerque[120] , D. Aleksandrov[88] , B. Alessandro[59] , R. Alfaro Molina[73] , Y. Ali[16] , A. Alici[11 ,54 ,29] , A. Alkin[3] , J. Alme[24] , T. Alt[70] , L. Altenkamper[24] , I. Altsybeev[138] , M.N. Anaam[7] , C. Andrei[48] , D. Andreou[36] , H.A. Andrews[108] , A. Andronic[142 ,104] , M. Angeletti[36] , V. Anguelov[102] , C. Anson[17] , T. Antičić[105] , F. Antinori[57] , P. Antonioli[54] , R. Anwar[124] , N. Apadula[80] , L. Aphecetche[112] , H. Appelshäuser[70] , S. Arcelli[29] , R. Arnaldi[59] , O.W. Arnold[103 ,115] , I.C. Arsene[23] , M. Arslandok[102] , B. Audurier[112] , A. Augustinus[36] , R. Averbeck[104] , M.D. Azmi[18] , A. Badalà[56] , Y.W. Baek[61 ,42] , S. Bagnasco[59] , R. Bailhache[70] , R. Bala[99] , A. Baldisseri[134] , M. Ball[44] , R.C. Baral[86] , A.M. Barbano[28] , R. Barbera[30] , F. Barile[53] , L. Barioglio[28] , G.G. Barnaföldi[143] , L.S. Barnby[93] , V. Barret[131] , P. Bartalini[7] , K. Barth[36] , E. Bartsch[70] , N. Bastid[131] , S. Basu[141] , G. Batigne[112] , B. Batyunya[76] , P.C. Batzing[23] , J.L. Bazo Alba[109] , I.G. Bearden[89] , H. Beck[102] , C. Bedda[64] , N.K. Behera[61] , I. Belikov[133] , F. Bellini[36] , H. Bello Martinez[2] , R. Bellwied[124] , L.G.E. Beltran[118] , V. Belyaev[92] , G. Bencedi[143] , S. Beole[28] , A. Bercuci[48] , Y. Berdnikov[96] , D. Berenyi[143] , R.A. Bertens[127] , D. Berzano[36 ,59] , L. Betev[36] , P.P. Bhaduri[139] , A. Bhasin[99] , I.R. Bhat[99] , H. Bhatt[49] , B. Bhattacharjee[43] , J. Bhom[116] , A. Bianchi[28] , L. Bianchi[124] , N. Bianchi[52] , J. Bielčík[39] , J. Bielčíková[94] , A. Bilandzic[115 ,103] , G. Biro[143] , R. Biswas[4] , S. Biswas[4] , J.T. Blair[117] , D. Blau[88] , C. Blume[70] , G. Boca[136] , F. Bock[36] , A. Bogdanov[92] , L. Boldizsár[143] , M. Bombara[40] , G. Bonomi[137] , M. Bonora[36] , H. Borel[134] , A. Borissov[20 ,142] , M. Borri[126] , E. Botta[28] , C. Bourjau[89] , L. Bratrud[70] , P. Braun-Munzinger[104] , M. Bregant[119] , T.A. Broker[70] , M. Broz[39] , E.J. Brucken[45] , E. Bruna[59] , G.E. Bruno[36 ,35] , D. Budnikov[106] , H. Buesching[70] , S. Bufalino[33] , P. Buhler[111] , P. Buncic[36] , O. Busch[130 , i] , Z. Buthelezi[74] , J.B. Butt[16] , J.T. Buxton[19] , J. Cabala[114] , D. Caffarri[90] , H. Caines[144] , A. Caliva[104] , E. Calvo Villar[109] , R.S. Camacho[2] , P. Camerini[27] , A.A. Capon[111] , F. Carena[36] , W. Carena[36] , F. Carnesecchi[29 ,11] , J. Castillo Castellanos[134] , A.J. Castro[127] , E.A.R. Casula[55] , C. Ceballos Sanchez[9] , S. Chandra[139] , B. Chang[125] , W. Chang[7] , S. Chapeland[36] , M. Chartier[126] , S. Chattopadhyay[139] , S. Chattopadhyay[107] , A. Chauvin[103 ,115] , C. Cheshkov[132] , B. Cheynis[132] , V. Chibante Barroso[36] , D.D. Chinellato[120] , S. Cho[61] , P. Chochula[36] , T. Chowdhury[131] , P. Christakoglou[90] , C.H. Christensen[89] , P. Christiansen[81] , T. Chujo[130] , S.U. Chung[20] , C. Cicalo[55] , L. Cifarelli[11 ,29] , F. Cindolo[54] , J. Cleymans[123] , F. Colamaria[53] , D. Colella[66 ,36 ,53] , A. Collu[80] , M. Colocci[29] , M. Concas[59 , ii] , G. Conesa Balbastre[79] , Z. Conesa del Valle[62] , J.G. Contreras[39] , T.M. Cormier[95] , Y. Corrales Morales[59] , P. Cortese[34] , M.R. Cosentino[121] , F. Costa[36] , S. Costanza[136] , J. Crkovská[62] , P. Crochet[131] , E. Cuautle[71] , L. Cunqueiro[142 ,95] , T. Dahms[103 ,115] , A. Dainese[57] , S. Dani[67] , M.C. Danisch[102] , A. Danu[69] , D. Das[107] , I. Das[107] , S. Das[4] , A. Dash[86] , S. Dash[49] , S. De[50] , A. De Caro[32] , G. de Cataldo[53] , C. de Conti[119] , J. de Cuveland[41] , A. De Falco[26] , D. De Gruttola[11 ,32] , N. De Marco[59] , S. De Pasquale[32] , R.D. De Souza[120] , H.F. Degenhardt[119] , A. Deisting[104 ,102] , A. Deloff[85] , S. Delsanto[28] , C. Deplano[90] , P. Dhankher[49] , D. Di Bari[35] , A. Di Mauro[36] , B. Di Ruzza[57] , R.A. Diaz[9] , T. Dietel[123] , P. Dillenseger[70] , Y. Ding[7] , R. Divià[36] , Ø. Djuvsland[24] , A. Dobrin[36] , D. Domenicis Gimenez[119] , B. Dönigus[70] , O. Dordic[23] , L.V.R. Doremalen[64] , A.K. Dubey[139] , A. Dubla[104] , L. Ducroux[132] , S. Dudi[98] , A.K. Duggal[98] , M. Dukhishyam[86] , P. Dupieux[131] , R.J. Ehlers[144] , D. Elia[53] , E. Endress[109] , H. Engel[75] , E. Epple[144] , B. Erazmus[112] , F. Erhardt[97] , M.R. Ersdal[24] , B. Espagnon[62] , G. Eulisse[36] , J. Eum[20] , D. Evans[108] , S. Evdokimov[91] , L. Fabbietti[103 ,115] , M. Faggin[31] , J. Faivre[79] , A. Fantoni[52] , M. Fasel[95] , L. Feldkamp[142] , A. Feliciello[59] , G. Feofilov[138] , A. Fernández Téllez[2] , A. Ferretti[28] ,

A. Festanti[31 ,36] , V.J.G. Feuillard[102] , J. Figiel[116] , M.A.S. Figueredo[119] , S. Filchagin[106] ,
D. Finogeev[63] , F.M. Fionda[24] , G. Fiorenza[53] , F. Flor[124] , M. Floris[36] , S. Foertsch[74] ,
P. Foka[104] , S. Fokin[88] , E. Fragiacomo[60] , A. Francescon[36] , A. Francisco[112] , U. Frankenfeld[104] ,
G.G. Fronze[28] , U. Fuchs[36] , C. Furget[79] , A. Furs[63] , M. Fusco Girard[32] , J.J. Gaardhøje[89] ,
M. Gagliardi[28] , A.M. Gago[109] , K. Gajdosova[89] , M. Gallio[28] , C.D. Galvan[118] , P. Ganoti[84] ,
C. Garabatos[104] , E. Garcia-Solis[12] , K. Garg[30] , C. Gargiulo[36] , P. Gasik[115 ,103] , E.F. Gauger[117] ,
M.B. Gay Ducati[72] , M. Germain[112] , J. Ghosh[107] , P. Ghosh[139] , S.K. Ghosh[4] , P. Gianotti[52] ,
P. Giubellino[104 ,59] , P. Giubilato[31] , P. Glässel[102] , D.M. Goméz Coral[73] , A. Gomez Ramirez[75] ,
V. Gonzalez[104] , P. González-Zamora[2] , S. Gorbunov[41] , L. Görlich[116] , S. Gotovac[37] ,
V. Grabski[73] , L.K. Graczykowski[140] , K.L. Graham[108] , L. Greiner[80] , A. Grelli[64] , C. Grigoras[36] ,
V. Grigoriev[92] , A. Grigoryan[1] , S. Grigoryan[76] , J.M. Gronefeld[104] , F. Grosa[33] ,
J.F. Grosse-Oetringhaus[36] , R. Grosso[104] , R. Guernane[79] , B. Guerzoni[29] , M. Guittiere[112] ,
K. Gulbrandsen[89] , T. Gunji[129] , A. Gupta[99] , R. Gupta[99] , I.B. Guzman[2] , R. Haake[36] ,
M.K. Habib[104] , C. Hadjidakis[62] , H. Hamagaki[82] , G. Hamar[143] , M. Hamid[7] , J.C. Hamon[133] ,
R. Hannigan[117] , M.R. Haque[64] , J.W. Harris[144] , A. Harton[12] , H. Hassan[79] ,
D. Hatzifotiadou[54 ,11] , S. Hayashi[129] , S.T. Heckel[70] , E. Hellbär[70] , H. Helstrup[38] ,
A. Herghelegiu[48] , E.G. Hernandez[2] , G. Herrera Corral[10] , F. Herrmann[142] , K.F. Hetland[38] ,
T.E. Hilden[45] , H. Hillemanns[36] , C. Hills[126] , B. Hippolyte[133] , B. Hohlweger[103] , D. Horak[39] ,
S. Hornung[104] , R. Hosokawa[130 ,79] , J. Hota[67] , P. Hristov[36] , C. Huang[62] , C. Hughes[127] ,
P. Huhn[70] , T.J. Humanic[19] , H. Hushnud[107] , N. Hussain[43] , T. Hussain[18] , D. Hutter[41] ,
D.S. Hwang[21] , J.P. Iddon[126] , S.A. Iga Buitron[71] , R. Ilkaev[106] , M. Inaba[130] , M. Ippolitov[88] ,
M.S. Islam[107] , M. Ivanov[104] , V. Ivanov[96] , V. Izucheev[91] , B. Jacak[80] , N. Jacazio[29] ,
P.M. Jacobs[80] , M.B. Jadhav[49] , S. Jadlovska[114] , J. Jadlovsky[114] , S. Jaelani[64] ,
C. Jahnke[119 ,115] , M.J. Jakubowska[140] , M.A. Janik[140] , C. Jena[86] , M. Jercic[97] , O. Jevons[108] ,
R.T. Jimenez Bustamante[104] , M. Jin[124] , P.G. Jones[108] , A. Jusko[108] , P. Kalinak[66] ,
A. Kalweit[36] , J.H. Kang[145] , V. Kaplin[92] , S. Kar[7] , A. Karasu Uysal[78] , O. Karavichev[63] ,
T. Karavicheva[63] , P. Karczmarczyk[36] , E. Karpechev[63] , U. Kebschull[75] , R. Keidel[47] ,
D.L.D. Keijdener[64] , M. Keil[36] , B. Ketzer[44] , Z. Khabanova[90] , A.M. Khan[7] , S. Khan[18] ,
S.A. Khan[139] , A. Khanzadeev[96] , Y. Kharlov[91] , A. Khatun[18] , A. Khuntia[50] ,
M.M. Kielbowicz[116] , B. Kileng[38] , B. Kim[130] , D. Kim[145] , D.J. Kim[125] , E.J. Kim[14] , H. Kim[145] ,
J.S. Kim[42] , J. Kim[102] , M. Kim[61 ,102] , S. Kim[21] , T. Kim[145] , T. Kim[145] , S. Kirsch[41] ,
I. Kisel[41] , S. Kiselev[65] , A. Kisiel[140] , J.L. Klay[6] , C. Klein[70] , J. Klein[36 ,59] , C. Klein-Bösing[142] ,
S. Klewin[102] , A. Kluge[36] , M.L. Knichel[36] , A.G. Knospe[124] , C. Kobdaj[113] , M. Kofarago[143] ,
M.K. Köhler[102] , T. Kollegger[104] , N. Kondratyeva[92] , E. Kondratyuk[91] , A. Konevskikh[63] ,
M. Konyushikhin[141] , O. Kovalenko[85] , V. Kovalenko[138] , M. Kowalski[116] , I. Králik[66] ,
A. Kravčáková[40] , L. Kreis[104] , M. Krivda[66 ,108] , F. Krizek[94] , M. Krüger[70] , E. Kryshen[96] ,
M. Krzewicki[41] , A.M. Kubera[19] , V. Kučera[94 ,61] , C. Kuhn[133] , P.G. Kuijer[90] , J. Kumar[49] ,
L. Kumar[98] , S. Kumar[49] , S. Kundu[86] , P. Kurashvili[85] , A. Kurepin[63] , A.B. Kurepin[63] ,
A. Kuryakin[106] , S. Kushpil[94] , J. Kvapil[108] , M.J. Kweon[61] , Y. Kwon[145] , S.L. La Pointe[41] ,
P. La Rocca[30] , Y.S. Lai[80] , I. Lakomov[36] , R. Langoy[122] , K. Lapidus[144] , C. Lara[75] ,
A. Lardeux[23] , P. Larionov[52] , E. Laudi[36] , R. Lavicka[39] , R. Lea[27] , L. Leardini[102] , S. Lee[145] ,
F. Lehas[90] , S. Lehner[111] , J. Lehrbach[41] , R.C. Lemmon[93] , I. León Monzón[118] , P. Lévai[143] ,
X. Li[13] , X.L. Li[7] , J. Lien[122] , R. Lietava[108] , B. Lim[20] , S. Lindal[23] , V. Lindenstruth[41] ,
S.W. Lindsay[126] , C. Lippmann[104] , M.A. Lisa[19] , V. Litichevskyi[45] , A. Liu[80] , H.M. Ljunggren[81] ,
W.J. Llope[141] , D.F. Lodato[64] , V. Loginov[92] , C. Loizides[95 ,80] , P. Loncar[37] , X. Lopez[131] ,
E. López Torres[9] , A. Lowe[143] , P. Luettig[70] , J.R. Luhder[142] , M. Lunardon[31] , G. Luparello[60] ,
M. Lupi[36] , A. Maevskaya[63] , M. Mager[36] , S.M. Mahmood[23] , A. Maire[133] , R.D. Majka[144] ,
M. Malaev[96] , Q.W. Malik[23] , L. Malinina[76 , iii] , D. Mal'Kevich[65] , P. Malzacher[104] ,

A. Mamonov[106] , V. Manko[88] , F. Manso[131] , V. Manzari[53] , Y. Mao[7] , M. Marchisone[128 ,74 ,132] ,
J. Mareš[68] , G.V. Margagliotti[27] , A. Margotti[54] , J. Margutti[64] , A. Marín[104] , C. Markert[117] ,
M. Marquard[70] , N.A. Martin[104] , P. Martinengo[36] , J.L. Martinez[124] , M.I. Martínez[2] ,
G. Martínez García[112] , M. Martinez Pedreira[36] , S. Masciocchi[104] , M. Masera[28] , A. Masoni[55] ,
L. Massacrier[62] , E. Masson[112] , A. Mastroserio[53 ,135] , A.M. Mathis[115 ,103] , P.F.T. Matuoka[119] ,
A. Matyja[116 ,127] , C. Mayer[116] , M. Mazzilli[35] , M.A. Mazzoni[58] , F. Meddi[25] , Y. Melikyan[92] ,
A. Menchaca-Rocha[73] , E. Meninno[32] , J. Mercado Pérez[102] , M. Meres[15] , C.S. Meza[109] ,
S. Mhlanga[123] , Y. Miake[130] , L. Micheletti[28] , M.M. Mieskolainen[45] , D.L. Mihaylov[103] ,
K. Mikhaylov[65 ,76] , A. Mischke[64] , A.N. Mishra[71] , D. Miśkowiec[104] , J. Mitra[139] , C.M. Mitu[69] ,
N. Mohammadi[36] , A.P. Mohanty[64] , B. Mohanty[86] , M. Mohisin Khan[18 , iv] , D.A. Moreira De
Godoy[142] , L.A.P. Moreno[2] , S. Moretto[31] , A. Morreale[112] , A. Morsch[36] , V. Muccifora[52] ,
E. Mudnic[37] , D. Mühlheim[142] , S. Muhuri[139] , M. Mukherjee[4] , J.D. Mulligan[144] ,
M.G. Munhoz[119] , K. Münning[44] , M.I.A. Munoz[80] , R.H. Munzer[70] , H. Murakami[129] ,
S. Murray[74] , L. Musa[36] , J. Musinsky[66] , C.J. Myers[124] , J.W. Myrcha[140] , B. Naik[49] , R. Nair[85] ,
B.K. Nandi[49] , R. Nania[54 ,11] , E. Nappi[53] , A. Narayan[49] , M.U. Naru[16] , A.F. Nassirpour[81] ,
H. Natal da Luz[119] , C. Nattrass[127] , S.R. Navarro[2] , K. Nayak[86] , R. Nayak[49] , T.K. Nayak[139] ,
S. Nazarenko[106] , R.A. Negrao De Oliveira[70 ,36] , L. Nellen[71] , S.V. Nesbo[38] , G. Neskovic[41] ,
F. Ng[124] , M. Nicassio[104] , J. Niedziela[140 ,36] , B.S. Nielsen[89] , S. Nikolaev[88] , S. Nikulin[88] ,
V. Nikulin[96] , F. Noferini[11 ,54] , P. Nomokonov[76] , G. Nooren[64] , J.C.C. Noris[2] , J. Norman[79] ,
A. Nyanin[88] , J. Nystrand[24] , H. Oh[145] , A. Ohlson[102] , J. Oleniacz[140] , A.C. Oliveira Da Silva[119] ,
M.H. Oliver[144] , J. Onderwaater[104] , C. Oppedisano[59] , R. Orava[45] , M. Oravec[114] , A. Ortiz
Velasquez[71] , A. Oskarsson[81] , J. Otwinowski[116] , K. Oyama[82] , Y. Pachmayer[102] , V. Pacik[89] ,
D. Pagano[137] , G. Paić[71] , P. Palni[7] , J. Pan[141] , A.K. Pandey[49] , S. Panebianco[134] ,
V. Papikyan[1] , P. Pareek[50] , J. Park[61] , J.E. Parkkila[125] , S. Parmar[98] , A. Passfeld[142] ,
S.P. Pathak[124] , R.N. Patra[139] , B. Paul[59] , H. Pei[7] , T. Peitzmann[64] , X. Peng[7] , L.G. Pereira[72] ,
H. Pereira Da Costa[134] , D. Peresunko[88] , E. Perez Lezama[70] , V. Peskov[70] , Y. Pestov[5] ,
V. Petráček[39] , M. Petrovici[48] , C. Petta[30] , R.P. Pezzi[72] , S. Piano[60] , M. Pikna[15] , P. Pillot[112] ,
L.O.D.L. Pimentel[89] , O. Pinazza[54 ,36] , L. Pinsky[124] , S. Pisano[52] , D.B. Piyarathna[124] ,
M. Płoskoń[80] , M. Planinic[97] , F. Pliquett[70] , J. Pluta[140] , S. Pochybova[143] ,
P.L.M. Podesta-Lerma[118] , M.G. Poghosyan[95] , B. Polichtchouk[91] , N. Poljak[97] ,
W. Poonsawat[113] , A. Pop[48] , H. Poppenborg[142] , S. Porteboeuf-Houssais[131] , V. Pozdniakov[76] ,
S.K. Prasad[4] , R. Preghenella[54] , F. Prino[59] , C.A. Pruneau[141] , I. Pshenichnov[63] , M. Puccio[28] ,
V. Punin[106] , J. Putschke[141] , S. Raha[4] , S. Rajput[99] , J. Rak[125] , A. Rakotozafindrabe[134] ,
L. Ramello[34] , F. Rami[133] , R. Raniwala[100] , S. Raniwala[100] , S.S. Räsänen[45] , B.T. Rascanu[70] ,
V. Ratza[44] , I. Ravasenga[33] , K.F. Read[127 ,95] , K. Redlich[85 , v] , A. Rehman[24] , P. Reichelt[70] ,
F. Reidt[36] , X. Ren[7] , R. Renfordt[70] , A. Reshetin[63] , J.-P. Revol[11] , K. Reygers[102] , V. Riabov[96] ,
T. Richert[64 ,81] , M. Richter[23] , P. Riedler[36] , W. Riegler[36] , F. Riggi[30] , C. Ristea[69] ,
S.P. Rode[50] , M. Rodríguez Cahuantzi[2] , K. Røed[23] , R. Rogalev[91] , E. Rogochaya[76] , D. Rohr[36] ,
D. Röhrich[24] , P.S. Rokita[140] , F. Ronchetti[52] , E.D. Rosas[71] , K. Roslon[140] , P. Rosnet[131] ,
A. Rossi[31] , A. Rotondi[136] , F. Roukoutakis[84] , C. Roy[133] , P. Roy[107] , O.V. Rueda[71] , R. Rui[27] ,
B. Rumyantsev[76] , A. Rustamov[87] , E. Ryabinkin[88] , Y. Ryabov[96] , A. Rybicki[116] , S. Saarinen[45] ,
S. Sadhu[139] , S. Sadovsky[91] , K. Šafařík[36] , S.K. Saha[139] , B. Sahoo[49] , P. Sahoo[50] , R. Sahoo[50] ,
S. Sahoo[67] , P.K. Sahu[67] , J. Saini[139] , S. Sakai[130] , M.A. Saleh[141] , S. Sambyal[99] ,
V. Samsonov[96 ,92] , A. Sandoval[73] , A. Sarkar[74] , D. Sarkar[139] , N. Sarkar[139] , P. Sarma[43] ,
M.H.P. Sas[64] , E. Scapparone[54] , F. Scarlassara[31] , B. Schaefer[95] , H.S. Scheid[70] , C. Schiaua[48] ,
R. Schicker[102] , C. Schmidt[104] , H.R. Schmidt[101] , M.O. Schmidt[102] , M. Schmidt[101] ,
N.V. Schmidt[95 ,70] , J. Schukraft[36] , Y. Schutz[36 ,133] , K. Schwarz[104] , K. Schweda[104] ,
G. Scioli[29] , E. Scomparin[59] , M. Šefčík[40] , J.E. Seger[17] , Y. Sekiguchi[129] , D. Sekihata[46] ,

I. Selyuzhenkov[104],[92], K. Senosi[74], S. Senyukov[133], E. Serradilla[73], P. Sett[49], A. Sevcenco[69], A. Shabanov[63], A. Shabetai[112], R. Shahoyan[36], W. Shaikh[107], A. Shangaraev[91], A. Sharma[98], A. Sharma[99], M. Sharma[99], N. Sharma[98], A.I. Sheikh[139], K. Shigaki[46], M. Shimomura[83], S. Shirinkin[65], Q. Shou[7],[110], K. Shtejer[28], Y. Sibiriak[88], S. Siddhanta[55], K.M. Sielewicz[36], T. Siemiarczuk[85], D. Silvermyr[81], G. Simatovic[90], G. Simonetti[36],[103], R. Singaraju[139], R. Singh[86], R. Singh[99], V. Singhal[139], T. Sinha[107], B. Sitar[15], M. Sitta[34], T.B. Skaali[23], M. Slupecki[125], N. Smirnov[144], R.J.M. Snellings[64], T.W. Snellman[125], J. Song[20], F. Soramel[31], S. Sorensen[127], F. Sozzi[104], I. Sputowska[116], J. Stachel[102], I. Stan[69], P. Stankus[95], E. Stenlund[81], D. Stocco[112], M.M. Storetvedt[38], P. Strmen[15], A.A.P. Suaide[119], T. Sugitate[46], C. Suire[62], M. Suleymanov[16], M. Suljic[36],[27], R. Sultanov[65], M. Šumbera[94], S. Sumowidagdo[51], K. Suzuki[111], S. Swain[67], A. Szabo[15], I. Szarka[15], U. Tabassam[16], J. Takahashi[120], G.J. Tambave[24], N. Tanaka[130], M. Tarhini[112], M. Tariq[18], M.G. Tarzila[48], A. Tauro[36], G. Tejeda Muñoz[2], A. Telesca[36], C. Terrevoli[31], B. Teyssier[132], D. Thakur[50], S. Thakur[139], D. Thomas[117], F. Thoresen[89], R. Tieulent[132], A. Tikhonov[63], A.R. Timmins[124], A. Toia[70], N. Topilskaya[63], M. Toppi[52], S.R. Torres[118], S. Tripathy[50], S. Trogolo[28], G. Trombetta[35], L. Tropp[40], V. Trubnikov[3], W.H. Trzaska[125], T.P. Trzcinski[140], B.A. Trzeciak[64], T. Tsuji[129], A. Tumkin[106], R. Turrisi[57], T.S. Tveter[23], K. Ullaland[24], E.N. Umaka[124], A. Uras[132], G.L. Usai[26], A. Utrobicic[97], M. Vala[114], J.W. Van Hoorne[36], M. van Leeuwen[64], P. Vande Vyvre[36], D. Varga[143], A. Vargas[2], M. Vargyas[125], R. Varma[49], M. Vasileiou[84], A. Vasiliev[88], A. Vauthier[79], O. Vázquez Doce[103],[115], V. Vechernin[138], A.M. Veen[64], E. Vercellin[28], S. Vergara Limón[2], L. Vermunt[64], R. Vernet[8], R. Vértesi[143], L. Vickovic[37], J. Viinikainen[125], Z. Vilakazi[128], O. Villalobos Baillie[108], A. Villatoro Tello[2], A. Vinogradov[88], T. Virgili[32], V. Vislavicius[89],[81], A. Vodopyanov[76], M.A. Völkl[101], K. Voloshin[65], S.A. Voloshin[141], G. Volpe[35], B. von Haller[36], I. Vorobyev[115],[103], D. Voscek[114], D. Vranic[104],[36], J. Vrláková[40], B. Wagner[24], H. Wang[64], M. Wang[7], Y. Watanabe[130], M. Weber[111], S.G. Weber[104], A. Wegrzynek[36], D.F. Weiser[102], S.C. Wenzel[36], J.P. Wessels[142], U. Westerhoff[142], A.M. Whitehead[123], J. Wiechula[70], J. Wikne[23], G. Wilk[85], J. Wilkinson[54], G.A. Willems[142],[36], M.C.S. Williams[54], E. Willsher[108], B. Windelband[102], W.E. Witt[127], R. Xu[7], S. Yalcin[78], K. Yamakawa[46], S. Yano[46], Z. Yin[7], H. Yokoyama[79],[130], I.-K. Yoo[20], J.H. Yoon[61], V. Yurchenko[3], V. Zaccolo[59], A. Zaman[16], C. Zampolli[36], H.J.C. Zanoli[119], N. Zardoshti[108], A. Zarochentsev[138], P. Závada[68], N. Zaviyalov[106], H. Zbroszczyk[140], M. Zhalov[96], X. Zhang[7], Y. Zhang[7], Z. Zhang[7],[131], C. Zhao[23], V. Zherebchevskii[138], N. Zhigareva[65], D. Zhou[7], Y. Zhou[89], Z. Zhou[24], H. Zhu[7], J. Zhu[7], Y. Zhu[7], A. Zichichi[29],[11], M.B. Zimmermann[36], G. Zinovjev[3], J. Zmeskal[111], S. Zou[7],

[i]   *Deceased*
[ii]   *Dipartimento DET del Politecnico di Torino, Turin, Italy*
[iii] *M.V. Lomonosov Moscow State University, D.V. Skobeltsyn Institute of Nuclear, Physics, Moscow, Russia*
[iv]   *Department of Applied Physics, Aligarh Muslim University, Aligarh, India*
[v]   *Institute of Theoretical Physics, University of Wroclaw, Poland*

[1] *A.I. Alikhanyan National Science Laboratory (Yerevan Physics Institute) Foundation, Yerevan, Armenia*
[2] *Benemérita Universidad Autónoma de Puebla, Puebla, Mexico*
[3] *Bogolyubov Institute for Theoretical Physics, National Academy of Sciences of Ukraine, Kiev, Ukraine*
[4] *Bose Institute, Department of Physics and Centre for Astroparticle Physics and Space Science (CAPSS), Kolkata, India*

[5]   *Budker Institute for Nuclear Physics, Novosibirsk, Russia*

[6]   *California Polytechnic State University, San Luis Obispo, California, United States*

[7]   *Central China Normal University, Wuhan, China*

[8]   *Centre de Calcul de l'IN2P3, Villeurbanne, Lyon, France*

[9]   *Centro de Aplicaciones Tecnológicas y Desarrollo Nuclear (CEADEN), Havana, Cuba*

[10] *Centro de Investigación y de Estudios Avanzados (CINVESTAV), Mexico City and Mérida, Mexico*

[11] *Centro Fermi — Museo Storico della Fisica e Centro Studi e Ricerche "Enrico Fermi", Rome, Italy*

[12] *Chicago State University, Chicago, Illinois, United States*

[13] *China Institute of Atomic Energy, Beijing, China*

[14] *Chonbuk National University, Jeonju, Republic of Korea*

[15] *Comenius University Bratislava, Faculty of Mathematics, Physics and Informatics, Bratislava, Slovakia*

[16] *COMSATS Institute of Information Technology (CIIT), Islamabad, Pakistan*

[17] *Creighton University, Omaha, Nebraska, United States*

[18] *Department of Physics, Aligarh Muslim University, Aligarh, India*

[19] *Department of Physics, Ohio State University, Columbus, Ohio, United States*

[20] *Department of Physics, Pusan National University, Pusan, Republic of Korea*

[21] *Department of Physics, Sejong University, Seoul, Republic of Korea*

[22] *Department of Physics, University of California, Berkeley, California, United States*

[23] *Department of Physics, University of Oslo, Oslo, Norway*

[24] *Department of Physics and Technology, University of Bergen, Bergen, Norway*

[25] *Dipartimento di Fisica dell'Università 'La Sapienza' and Sezione INFN, Rome, Italy*

[26] *Dipartimento di Fisica dell'Università and Sezione INFN, Cagliari, Italy*

[27] *Dipartimento di Fisica dell'Università and Sezione INFN, Trieste, Italy*

[28] *Dipartimento di Fisica dell'Università and Sezione INFN, Turin, Italy*

[29] *Dipartimento di Fisica e Astronomia dell'Università and Sezione INFN, Bologna, Italy*

[30] *Dipartimento di Fisica e Astronomia dell'Università and Sezione INFN, Catania, Italy*

[31] *Dipartimento di Fisica e Astronomia dell'Università and Sezione INFN, Padova, Italy*

[32] *Dipartimento di Fisica 'E.R. Caianiello' dell'Università and Gruppo Collegato INFN, Salerno, Italy*

[33] *Dipartimento DISAT del Politecnico and Sezione INFN, Turin, Italy*

[34] *Dipartimento di Scienze e Innovazione Tecnologica dell'Università del Piemonte Orientale and INFN Sezione di Torino, Alessandria, Italy*

[35] *Dipartimento Interateneo di Fisica 'M. Merlin' and Sezione INFN, Bari, Italy*

[36] *European Organization for Nuclear Research (CERN), Geneva, Switzerland*

[37] *Faculty of Electrical Engineering, Mechanical Engineering and Naval Architecture, University of Split, Split, Croatia*

[38] *Faculty of Engineering and Science, Western Norway University of Applied Sciences, Bergen, Norway*

[39] *Faculty of Nuclear Sciences and Physical Engineering, Czech Technical University in Prague, Prague, Czech Republic*

[40] *Faculty of Science, P.J. Šafárik University, Košice, Slovakia*

[41] *Frankfurt Institute for Advanced Studies, Johann Wolfgang Goethe-Universität Frankfurt, Frankfurt, Germany*

[42] *Gangneung-Wonju National University, Gangneung, Republic of Korea*

[43] *Gauhati University, Department of Physics, Guwahati, India*

[44] *Helmholtz-Institut für Strahlen- und Kernphysik, Rheinische Friedrich-Wilhelms-Universität Bonn, Bonn, Germany*

[45] *Helsinki Institute of Physics (HIP), Helsinki, Finland*

[46] *Hiroshima University, Hiroshima, Japan*

[47] *Hochschule Worms, Zentrum für Technologietransfer und Telekommunikation (ZTT), Worms, Germany*

[48] *Horia Hulubei National Institute of Physics and Nuclear Engineering, Bucharest, Romania*

49   *Indian Institute of Technology Bombay (IIT), Mumbai, India*
50   *Indian Institute of Technology Indore, Indore, India*
51   *Indonesian Institute of Sciences, Jakarta, Indonesia*
52   *INFN, Laboratori Nazionali di Frascati, Frascati, Italy*
53   *INFN, Sezione di Bari, Bari, Italy*
54   *INFN, Sezione di Bologna, Bologna, Italy*
55   *INFN, Sezione di Cagliari, Cagliari, Italy*
56   *INFN, Sezione di Catania, Catania, Italy*
57   *INFN, Sezione di Padova, Padova, Italy*
58   *INFN, Sezione di Roma, Rome, Italy*
59   *INFN, Sezione di Torino, Turin, Italy*
60   *INFN, Sezione di Trieste, Trieste, Italy*
61   *Inha University, Incheon, Republic of Korea*
62   *Institut de Physique Nucléaire d'Orsay (IPNO), Institut National de Physique Nucléaire et de Physique des Particules (IN2P3/CNRS), Université de Paris-Sud, Université Paris-Saclay, Orsay, France*
63   *Institute for Nuclear Research, Academy of Sciences, Moscow, Russia*
64   *Institute for Subatomic Physics, Utrecht University/Nikhef, Utrecht, Netherlands*
65   *Institute for Theoretical and Experimental Physics, Moscow, Russia*
66   *Institute of Experimental Physics, Slovak Academy of Sciences, Košice, Slovakia*
67   *Institute of Physics, Bhubaneswar, India*
68   *Institute of Physics of the Czech Academy of Sciences, Prague, Czech Republic*
69   *Institute of Space Science (ISS), Bucharest, Romania*
70   *Institut für Kernphysik, Johann Wolfgang Goethe-Universität Frankfurt, Frankfurt, Germany*
71   *Instituto de Ciencias Nucleares, Universidad Nacional Autónoma de México, Mexico City, Mexico*
72   *Instituto de Física, Universidade Federal do Rio Grande do Sul (UFRGS), Porto Alegre, Brazil*
73   *Instituto de Física, Universidad Nacional Autónoma de México, Mexico City, Mexico*
74   *iThemba LABS, National Research Foundation, Somerset West, South Africa*
75   *Johann-Wolfgang-Goethe Universität Frankfurt Institut für Informatik, Fachbereich Informatik und Mathematik, Frankfurt, Germany*
76   *Joint Institute for Nuclear Research (JINR), Dubna, Russia*
77   *Korea Institute of Science and Technology Information, Daejeon, Republic of Korea*
78   *KTO Karatay University, Konya, Turkey*
79   *Laboratoire de Physique Subatomique et de Cosmologie, Université Grenoble-Alpes, CNRS-IN2P3, Grenoble, France*
80   *Lawrence Berkeley National Laboratory, Berkeley, California, United States*
81   *Lund University Department of Physics, Division of Particle Physics, Lund, Sweden*
82   *Nagasaki Institute of Applied Science, Nagasaki, Japan*
83   *Nara Women's University (NWU), Nara, Japan*
84   *National and Kapodistrian University of Athens, School of Science, Department of Physics , Athens, Greece*
85   *National Centre for Nuclear Research, Warsaw, Poland*
86   *National Institute of Science Education and Research, HBNI, Jatni, India*
87   *National Nuclear Research Center, Baku, Azerbaijan*
88   *National Research Centre Kurchatov Institute, Moscow, Russia*
89   *Niels Bohr Institute, University of Copenhagen, Copenhagen, Denmark*
90   *Nikhef, National institute for subatomic physics, Amsterdam, Netherlands*
91   *NRC Kurchatov Institute IHEP, Protvino, Russia*
92   *NRNU Moscow Engineering Physics Institute, Moscow, Russia*
93   *Nuclear Physics Group, STFC Daresbury Laboratory, Daresbury, United Kingdom*
94   *Nuclear Physics Institute of the Czech Academy of Sciences, Řež u Prahy, Czech Republic*
95   *Oak Ridge National Laboratory, Oak Ridge, Tennessee, United States*
96   *Petersburg Nuclear Physics Institute, Gatchina, Russia*

97   *Physics department, Faculty of science, University of Zagreb, Zagreb, Croatia*
98   *Physics Department, Panjab University, Chandigarh, India*
99   *Physics Department, University of Jammu, Jammu, India*
100   *Physics Department, University of Rajasthan, Jaipur, India*
101   *Physikalisches Institut, Eberhard-Karls-Universität Tübingen, Tübingen, Germany*
102   *Physikalisches Institut, Ruprecht-Karls-Universität Heidelberg, Heidelberg, Germany*
103   *Physik Department, Technische Universität München, Munich, Germany*
104   *Research Division and ExtreMe Matter Institute EMMI, GSI Helmholtzzentrum für
      Schwerionenforschung GmbH, Darmstadt, Germany*
105   *Rudjer Bošković Institute, Zagreb, Croatia*
106   *Russian Federal Nuclear Center (VNIIEF), Sarov, Russia*
107   *Saha Institute of Nuclear Physics, Kolkata, India*
108   *School of Physics and Astronomy, University of Birmingham, Birmingham, United Kingdom*
109   *Sección Física, Departamento de Ciencias, Pontificia Universidad Católica del Perú, Lima, Peru*
110   *Shanghai Institute of Applied Physics, Shanghai, China*
111   *Stefan Meyer Institut für Subatomare Physik (SMI), Vienna, Austria*
112   *SUBATECH, IMT Atlantique, Université de Nantes, CNRS-IN2P3, Nantes, France*
113   *Suranaree University of Technology, Nakhon Ratchasima, Thailand*
114   *Technical University of Košice, Košice, Slovakia*
115   *Technische Universität München, Excellence Cluster 'Universe', Munich, Germany*
116   *The Henryk Niewodniczanski Institute of Nuclear Physics, Polish Academy of Sciences, Cracow,
      Poland*
117   *The University of Texas at Austin, Austin, Texas, United States*
118   *Universidad Autónoma de Sinaloa, Culiacán, Mexico*
119   *Universidade de São Paulo (USP), São Paulo, Brazil*
120   *Universidade Estadual de Campinas (UNICAMP), Campinas, Brazil*
121   *Universidade Federal do ABC, Santo Andre, Brazil*
122   *University College of Southeast Norway, Tonsberg, Norway*
123   *University of Cape Town, Cape Town, South Africa*
124   *University of Houston, Houston, Texas, United States*
125   *University of Jyväskylä, Jyväskylä, Finland*
126   *University of Liverpool, Department of Physics Oliver Lodge Laboratory , Liverpool, United
      Kingdom*
127   *University of Tennessee, Knoxville, Tennessee, United States*
128   *University of the Witwatersrand, Johannesburg, South Africa*
129   *University of Tokyo, Tokyo, Japan*
130   *University of Tsukuba, Tsukuba, Japan*
131   *Université Clermont Auvergne, CNRS/IN2P3, LPC, Clermont-Ferrand, France*
132   *Université de Lyon, Université Lyon 1, CNRS/IN2P3, IPN-Lyon, Villeurbanne, Lyon, France*
133   *Université de Strasbourg, CNRS, IPHC UMR 7178, F-67000 Strasbourg, France, Strasbourg, France*
134   *Université Paris-Saclay Centre d'Études de Saclay (CEA), IRFU, Department de Physique
      Nucléaire (DPhN), Saclay, France*
135   *Università degli Studi di Foggia, Foggia, Italy*
136   *Università degli Studi di Pavia, Pavia, Italy*
137   *Università di Brescia, Brescia, Italy*
138   *V. Fock Institute for Physics, St. Petersburg State University, St. Petersburg, Russia*
139   *Variable Energy Cyclotron Centre, Kolkata, India*
140   *Warsaw University of Technology, Warsaw, Poland*
141   *Wayne State University, Detroit, Michigan, United States*
142   *Westfälische Wilhelms-Universität Münster, Institut für Kernphysik, Münster, Germany*
143   *Wigner Research Centre for Physics, Hungarian Academy of Sciences, Budapest, Hungary*
144   *Yale University, New Haven, Connecticut, United States*
145   *Yonsei University, Seoul, Republic of Korea*